Constraints on parameters of dark matter and black hole in the Galactic Center

Alexander F. Zakharov
Institute of Theoretical and Experimental Physics, Moscow, Russia
BLTP, Joint Institute for Nuclear Research, Dubna, Russia
e-mail:zakharov@itep.ru

Scientific Session–Conference on Physics of Fundamental Interactions
Nuclear Physics Section of the Division of Physical Sciences of Russian Academy of Sciences
IHEP, Protvino, 22 December 2008

Outline of the talk

- Introduction
- Dark matter discovery
- 1998 – a sunrise of the precise cosmology era (in the beginning of the year the Universe was opened (N. Bahcall et al.) but at the end it was flat (SNe Ia data)
- Dichotomy: Searches for undiscovered DM and DE or alternative gravity law
- Hypothesis on Dark Matter Concentration near the Galactic Center

- Limits on Dark Matter Concentrations from Total Gravitating Mass Estimates
- Apocenter Shift Constraints: a Next Step Further
- Conclusions

Introduction

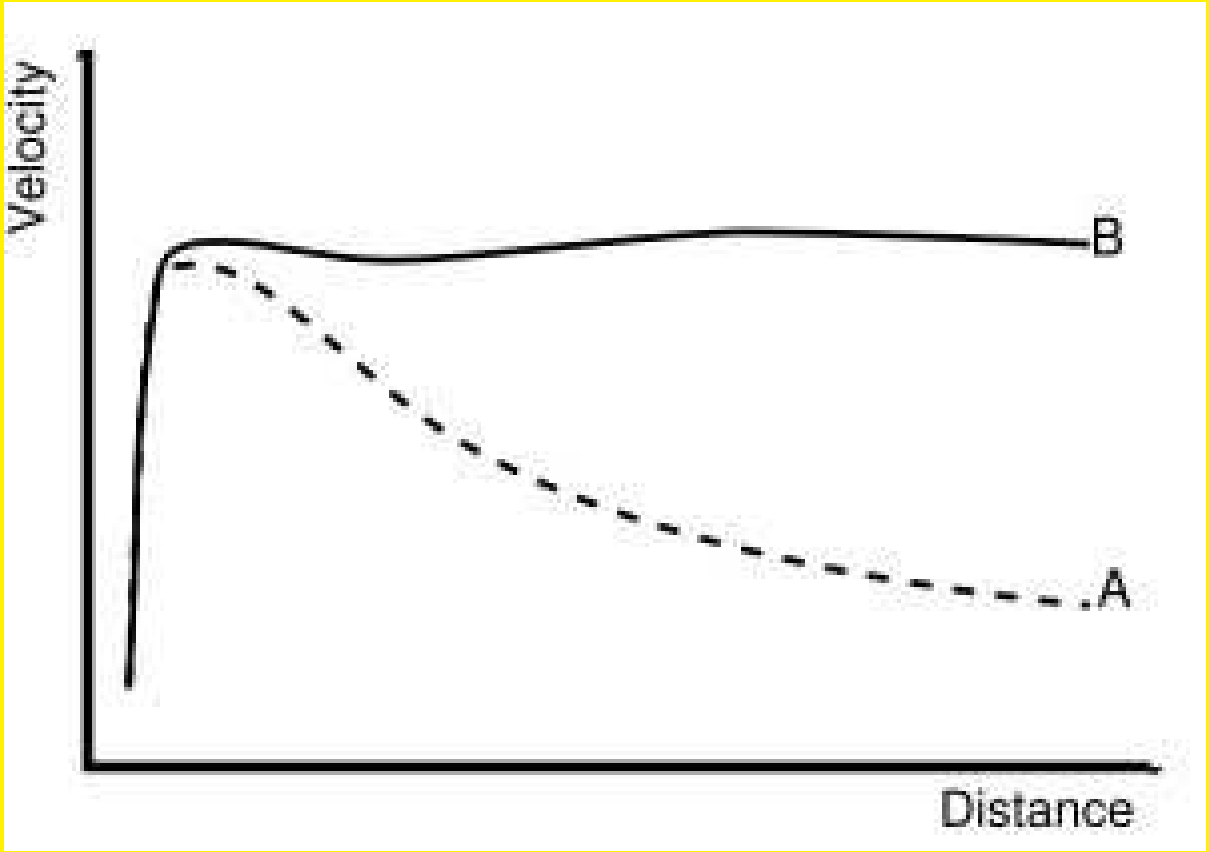

Figure 1: The DM evidence from rotation curves (it was established in 1970s (Rubin et al. (1970,1980...) and it was suspected in 1930s (Zwicky (1933,1937), Oort (1932)...))

From observations of the radial velocities of eight galaxies in the Coma cluster Zwicky (1933) found an unexpectedly large velocity dispersion $< v >= 1019 \pm 360 \ \mathrm{km/s}$. Zwicky concluded from that the mean density of the Coma cluster would have to be 400 times greater than that which is derived from luminous matter. Zwicky overestimated the mass-to-light ratio of the Coma cluster because he assumed a Hubble parameter $H_0 = 558 \ \mathrm{km/(s * Mpc)}$. His value for the high density of the Coma cluster should therefore be reduced from 400 to 50.

Zwicky: If this [high density] is confirmed we would arrive at the astonishing conclusion that dark matter is present [in Coma] with a much greater density than luminous matter.

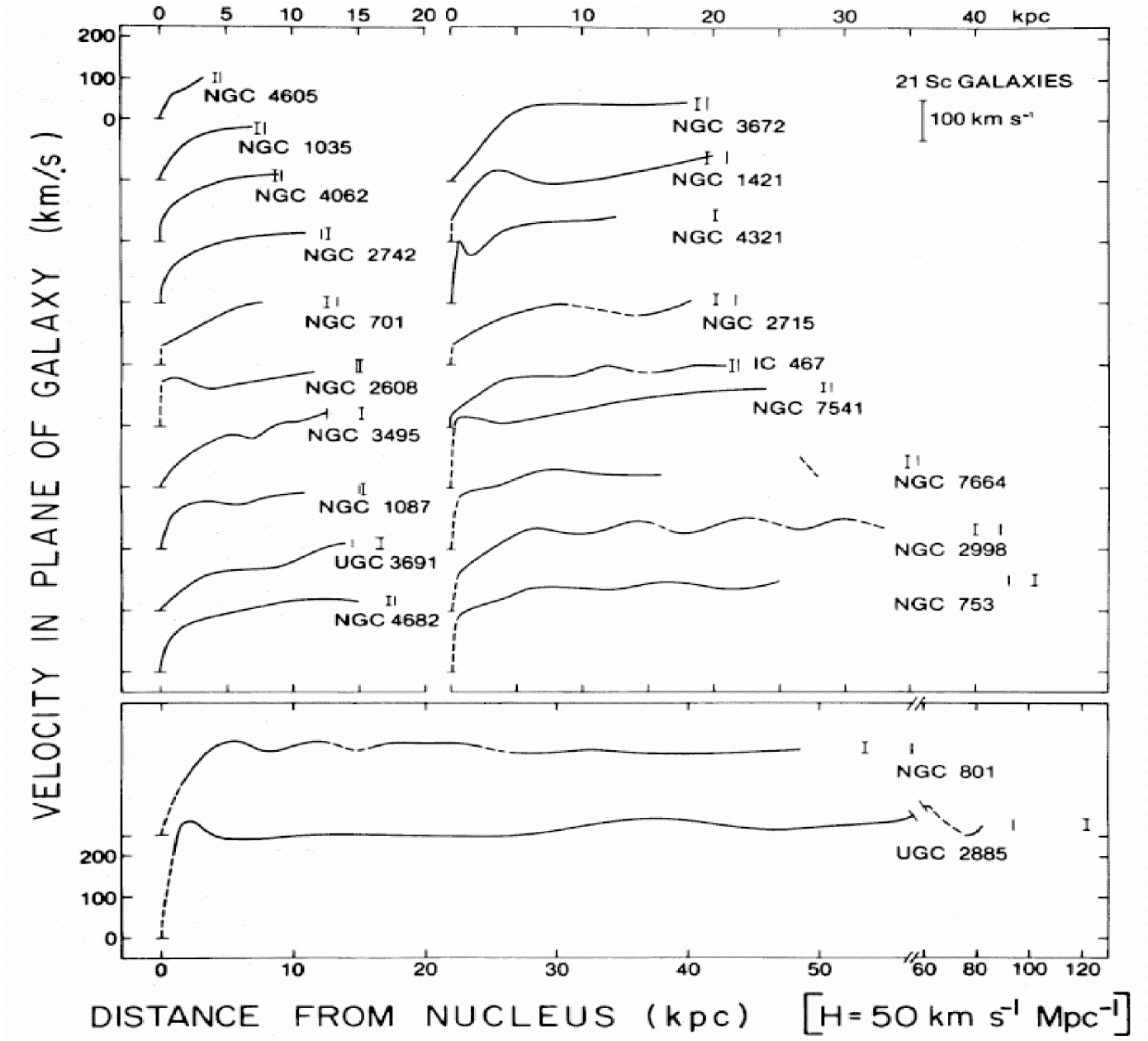

Figure 2: The DM evidence from rotation curves (Rubin et al. (1980)).)

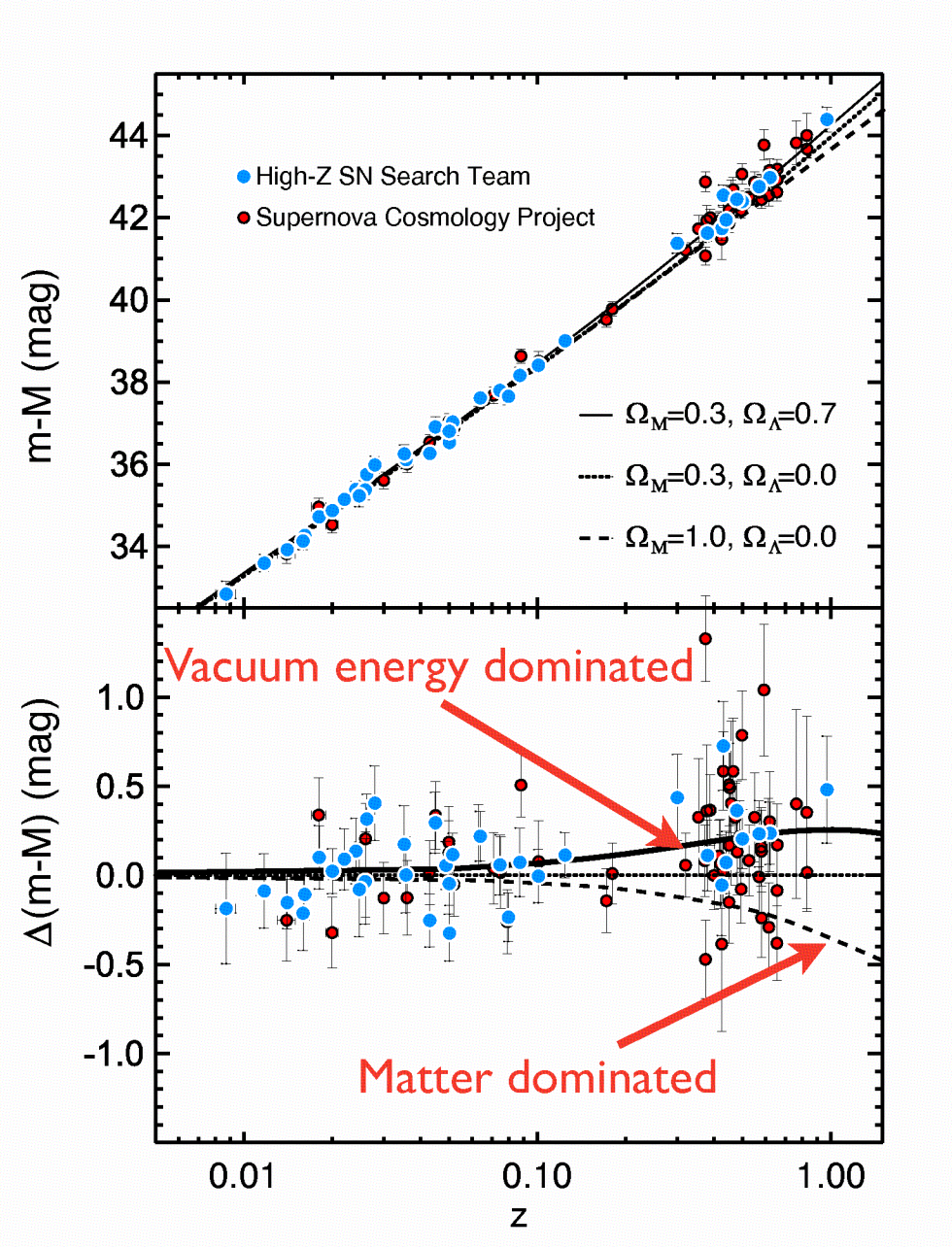

Figure 3: SNe Ia data in 1998

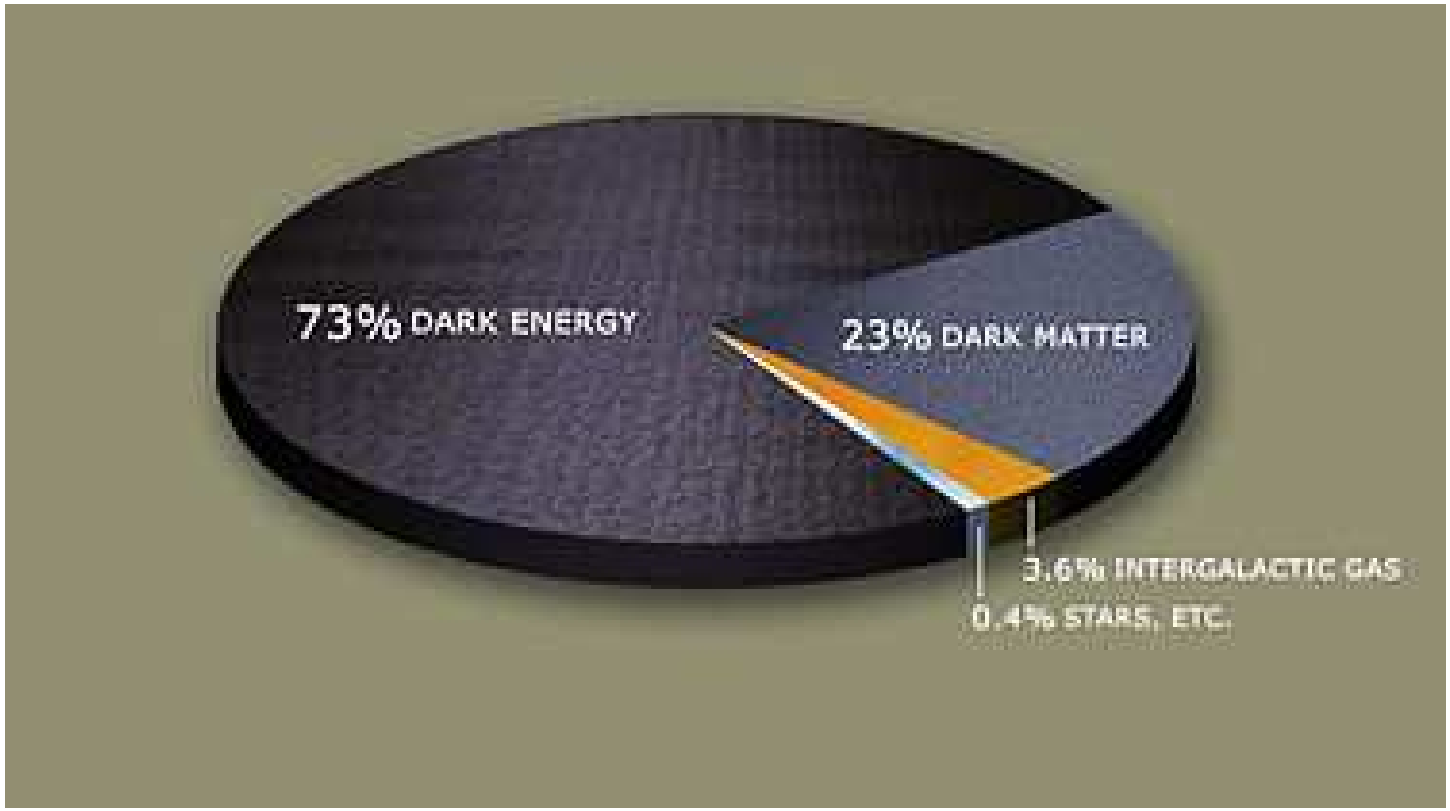

Figure 4: The components of the Universe (DE existence was suspected in 1980s).

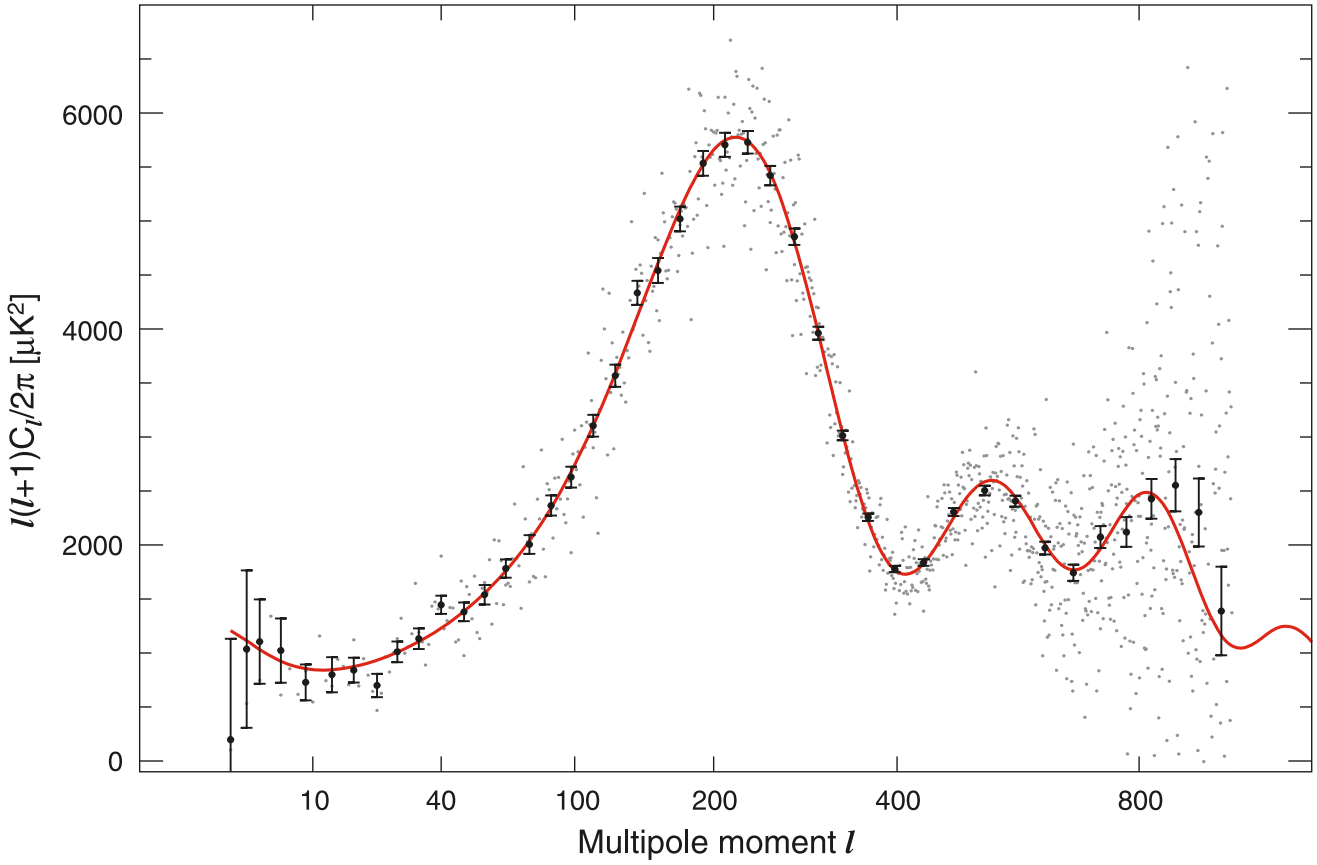

Fig. 5.— The temperature angular power spectrum corresponding to the *WMAP*-only best-fit ΛCDM model. The grey dots are the unbinned data; the black data points are binned data with 1σ error bars including both noise and cosmic variance computed for the best-fit model.

-2.5, $z_r < 30$ and impose positivity priors on r, α_{-1}, α_0, ω_ν, Y_p, and Ω_Λ, as well as requiring $0 < x_e < 1$. The tensor spectral index is fixed at $n_t = -r/8$. We place a prior on the Hubble constant of $20 < H_0 < 100$

Parameter	3 Year Mean	5 Year Mean	5 Year Max Like
$100\Omega_b h^2$	2.229 ± 0.073	2.273 ± 0.062	2.27
$\Omega_c h^2$	0.1054 ± 0.0078	0.1099 ± 0.0062	0.108
Ω_Λ	0.759 ± 0.034	0.742 ± 0.030	0.751
n_s	0.958 ± 0.016	$0.963^{+0.014}_{-0.015}$	0.961
τ	0.089 ± 0.030	0.087 ± 0.017	0.089
$\Delta^2_{\mathcal{R}}$	$(2.35 \pm 0.13) \times 10^{-9}$	$(2.41 \pm 0.11) \times 10^{-9}$	2.41×10^{-9}
σ_8	0.761 ± 0.049	0.796 ± 0.036	0.787
Ω_m	0.241 ± 0.034	0.258 ± 0.030	0.249
$\Omega_m h^2$	0.128 ± 0.008	0.1326 ± 0.0063	0.131
H_0	$73.2^{+3.1}_{-3.2}$	$71.9^{+2.6}_{-2.7}$	72.4
$z_{\rm reion}$	11.0 ± 2.6	11.0 ± 1.4	11.2
t_0	13.73 ± 0.16	13.69 ± 0.13	13.7

Table 2: ΛCDM model parameters and 68% confidence intervals from the five-year *WMAP* data alone. The three-year values are shown for comparison. For best estimates of parameters, the marginalized 'Mean' values should be used. The 'Max Like' values correspond to the single model giving the highest likelihood.

4. The ΛCDM Cosmological Model

4.1. *WMAP* five-year parameters

The ΛCDM model, described by just six parameters, is still an excellent fit to the *WMAP* data. The

DM searches

- Underground searches: DAMA, Edelweiss, CDMS... (Is DAMA right?)
- Indirect searches (neutralino annihilation): unresolved EGRET sources, neutralino stars, dark stars
- HEAT and PAMELA observations of relative number of positrons (a confirmation of Bergstrom et al. prediction or not?)
- Bullet cluster: the final proof or the challenge for alternative theories?
- Alternative theories (MOND (Milgrom), TeVeS (Bekenstein), gravitational polarization (Blanchet)...)

- WIMPs & LHC (an opportunity to discover neutralino)
- γ-radiation from the Galactic Center

10-point test (Taoso, Bertone and Masiero, 2008)

1. Does it match the appropriate relic density?
2. Is it cold?
3. Is it neutral?
4. Is it consistent with BBN?
5. Does it leave stellar evolution unchanged?
6. Is it compatible with constraints on self-interactions?
7. Is it consistent with direct DM searches?
8. Is it compatible with gamma-ray constraints?

9. Is it compatible with other astrophysical bounds?

10. Can it be probed experimentally?

EGRET diffuse radiation as a signal of neutralino annihilation

EGRET Excess of Diffuse Galactic Gamma Rays Interpreted as a Signal of Dark Matter Annihilation

Elsässer and Mannheim [1] fit a contribution of dark matter annihilation (DMA) to the *extragalactic* contribution of the galactic diffuse gamma ray flux, as deduced from the EGRET data by Strong, Moskalenko, and Reimer [2].

They find a weakly interacting massive particle (WIMP) mass of 515^{+110}_{-75} GeV and quote a systematic error of 30%. However, they do not include large systematic uncertainties from the fact that the determination of the extragalactic flux (EGF) requires a model for the subtraction of the galactic flux from the data. The data used were obtained with a model without galactic DMA, so one expects additional uncertainty in the region where DMA contributes. This is demonstrated in Fig. 1, where the EGF is obtained by subtracting the galactic contribution *including* the contribution from DMA [3]. The latter was determined from the excess of the EGRET data above the background from nuclear interactions in all sky directions, which allows one to obtain a parametrization of the halo profile. This halo profile was shown to describe the peculiar shape of the rotation curve of our galaxy [4], thus proving that the galactic excess of EGRET data traces the DM. With this DM halo profile the total Galactic flux including DMA can be calculated in all directions and subtracted from the EGRET data using the pioneering method of Sreekumar *et al.* [5]. This procedure was repeated for 8 different energy bins and the results are plotted in Fig. 1. As expected, the high energy tail differs considerably from Ref. [2] and can be either fitted with a simple power law, which yields a χ^2/d.o.f. of 10.9/6 or a probability of 9%, or by a double power law plus a contribution from DMA with a WIMP mass of 50 GeV, which yields a χ^2/d.o.f. of 4.7/4 or a probability of 31%. For the latter fit the shape of DMA was taken from Ref. [4] and the shape of the remaining contribution of the EGF could be fitted with a double power law, typical of many point sources. Both probabilities are acceptable, so there is no evidence for a signal of DMA in the *extragalactic* flux, but, on the other hand, a WIMP mass of 50 GeV is certainly acceptable and compatible with the excess in the *galactic* data [4], but incompatible with the value given in Ref. [1].

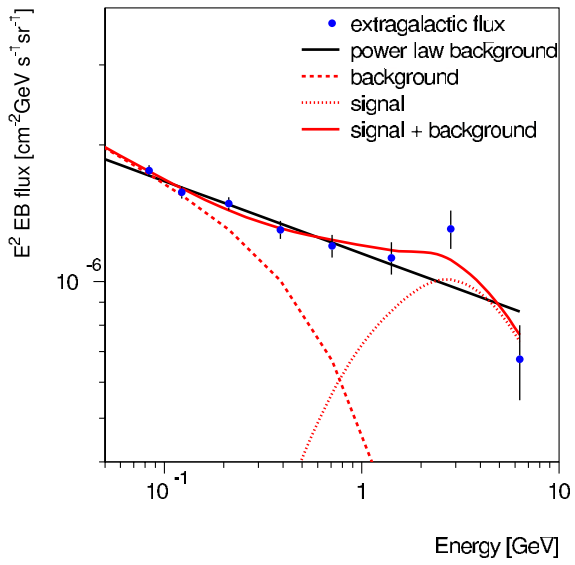

W. de Boer,* C. Sander, and V. Zhukov
Institut für Experimentelle Kernphysik
Universität Karlsruhe (TH)
P.O. Box 6980
76128 Karlsruhe, Germany

A. V. Gladyshev and D. I. Kazakov
Bogoliubov Laboratory of Theoretical Physics
Joint Institute for Nuclear Research
141 980 Dubna, Moscow Region, Russia

Received 14 June 2005; published 11 November 2005
DOI: 10.1103/PhysRevLett.95.209001
PACS numbers: 95.35.+d, 12.60.Jv, 98.70.Rz, 98.80.Cq

*Electronic address: Wim.de.Boer@cern.ch

[1] D. Elsässer and K. Mannheim, Phys. Rev. Lett. **94**, 171302 (2005).
[2] A. W. Strong, I. V. Moskalenko, and O. Reimer,

PAMELA & Searches for DM signatures

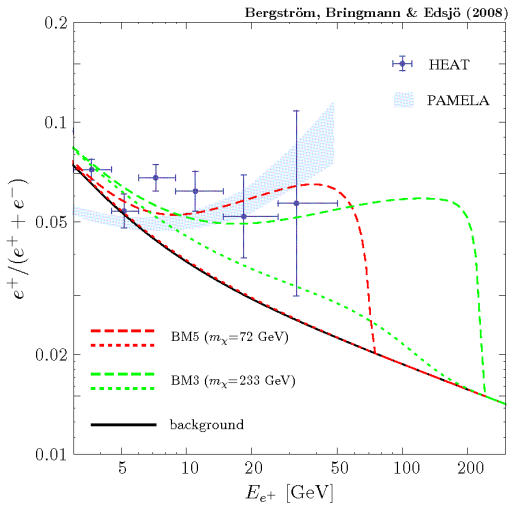

FIG. 3: The solid line is the expected flux ratio $e^+/(e^+ + e^-)$ as calculated following [32]. The data points are the combined HEAT data [33] and the light shaded area roughly corresponds to the (so far unpublished) PAMELA data [5]. Furthermore, the expected flux ratio for our benchmark models is shown without (dotted lines) and after taking into account radiative corrections (dashed lines). See text for further details.

Bullet cluster (1E0657-558 (z = 0.296)), Clowe et al. (2006)

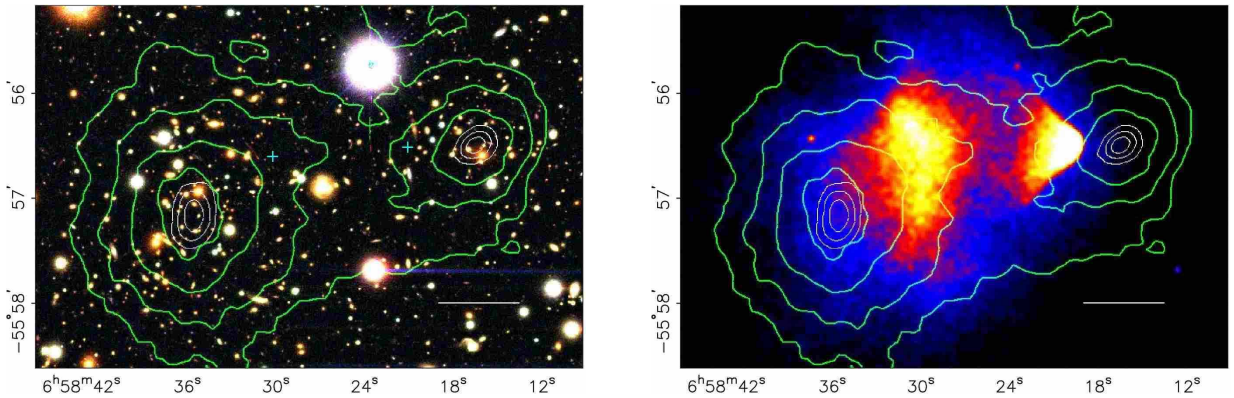

FIG. 1.— Shown above in the top panel is a color image from the Magellan images of the merging cluster 1E0657−558, with the white bar indicating 200 kpc at the distance of the cluster. In the bottom panel is a 500 ks Chandra image of the cluster. Shown in green contours in both panels are the weak lensing κ reconstruction with the outer contour level at $\kappa = 0.16$ and increasing in steps of 0.07. The white contours show the errors on the positions of the κ peaks and correspond to 68.3%, 95.5%, and 99.7% confidence levels. The blue +s show the location of the centers used to measure the masses of the plasma clouds in Table 2.

nated by collisionless dark matter, the potential will trace the distribution of that component, which is expected to be spatially coincident with the collisionless galaxies. Thus, by deriving a map of the gravitational potential, one can discriminate between these possibilities. We published an initial attempt at this using an archival VLT image (Clowe et al. 2004); here we add three additional optical image sets which allows us to increase the significance of the weak lensing results by more than a factor of 3.

In this paper, we measure distances at the redshift of the cluster, $z = 0.296$, by assuming an $\Omega_{\rm m} = 0.3, \lambda = 0.7, H_0 = 70$km/s/Mpc cosmology which results in 4.413 kpc/$''$ plate-scale. None of the results of this paper are dependent on this assumption; changing the assumed cosmology will result in a change of the distances and absolute masses measured, but the relative masses of the various structures in each measurement remain unchanged.

2. METHODOLOGY AND DATA

We construct a map of the gravitational potential using weak gravitational lensing (Mellier 1999; Bartelmann & Schneider 2001), which measures the distortions of images of background galaxies caused by the gravitational deflection of light by the cluster's mass. gravity, κ is equal to the surface mass density of the lens divided by a scaling constant. In non-standard gravity models, κ is no longer linearly related to the surface density but is instead a non-local function that scales as the mass raised to a power less than one for a planar lens, reaching the limit of one half for constant acceleration (Mortlock & Turner 2001; Zhao et al. 2006). While one can no longer directly obtain a map of the surface mass density using the distribution of κ in non-standard gravity models, the locations of the κ peaks, after adjusting for the extended wings, correspond to the locations of the surface mass density peaks.

Our goal is thus to obtain a map of κ. One can combine derivatives of $\vec{g}$ to obtain (Schneider 1995; Kaiser 1995)

$$\nabla \ln(1-\kappa) = \frac{1}{1-g_1^2-g_2^2} \begin{pmatrix} 1+g_1 & g_2 \\ g_2 & 1-g_1 \end{pmatrix} \begin{pmatrix} g_{1,1}+g_{2,2} \\ g_{2,1}-g_{1,2} \end{pmatrix},$$

which is integrated over the data field and converted into a two-dimensional map of κ. The observationally unconstrained constant of integration, typically referred to as the "mass-sheet degeneracy," is effectively the true mean of $\ln(1-\kappa)$ at the edge of the reconstruction. This method does, however, systematically underestimate κ in the cores of massive clusters. This results in a slight increase to the centroiding errors of the peaks, and our measurements of κ in the peaks of the components are

Bullet cluster (1E0657-558 ($z = 0.296$)), Angus et al. (2006)

TABLE 1
BEST FIT PARAMETERS OF THE CONVERGENCE MAP. SQUARED VELOCITIES IN $10^5(\mathrm{km\,s^{-1}})^2$ AND SCALE RADII, P, IN KPC (THE m INDEX STANDS FOR THE MAIN CLUSTER, THE s INDEX FOR THE SUB-CLUSTER).

$v^2_{m,gal}$	$v^2_{s,gal}$	$v^2_{m,x-ray}$	$v^2_{s,x-ray}$	$p_{m,gal}$	$p_{s,gal}$	$p_{m,x-ray}$	$p_{s,x-ray}$
28.4	14.5	3.8	1.7	227.4	155.4	62.6	33.4
$X_{m,gal}$	$Y_{m,gal}$	$X_{m,x-ray}$	$Y_{M,x-ray}$	$X_{s,gal}$	$Y_{s,gal}$	$X_{s,x-ray}$	$Y_{s,x-ray}$
-416.7	-173.1	-209.0	1.2	293.0	-2.7	147.5	3.6

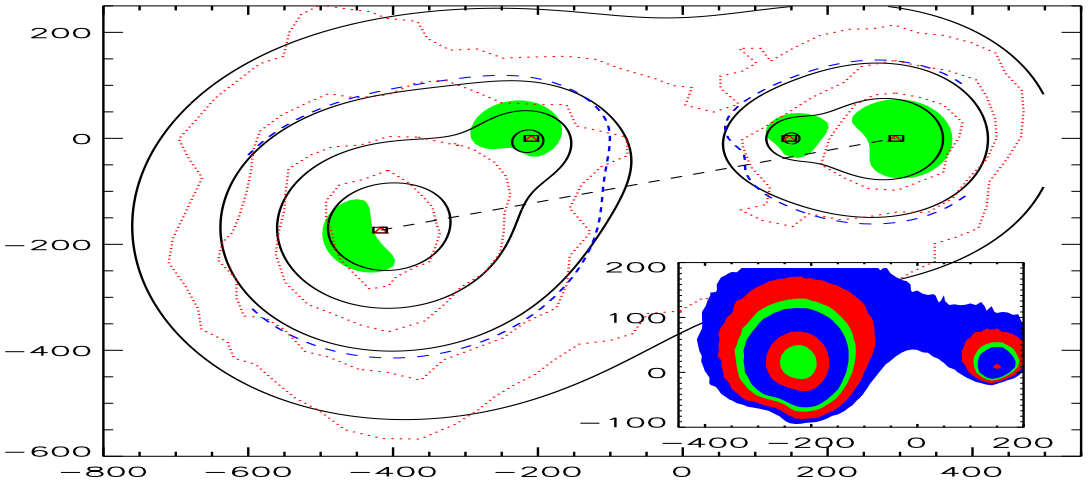

FIG. 1.— Our fitted convergence map (solid black lines) overplotted on the convergence map of C06 (dotted red lines) with x and y axes in kpc. The contours are from the outside 0.16,0.23,0.3 and 0.37. The most likely positions of the four potential centres are plotted with the black squares whereas the centres we used are the red triangles. Also overplotted (blue dashed line) is a contour of surface density $5 \times 10^6 M_\odot\,\mathrm{kpc}^{-2}$ for the MOND simple μ function; note slight distortion compared to the contour of kappa. The green shaded region is where matter density is above $1.8 \times 10^6 M_\odot\,\mathrm{kpc}^{-3}$ and correspond to the clustering of 2eV neutrinos.
inset: The surface density of the gas in the bullet cluster predicted by our DM subtraction method for the simple μ-function. The contour levels are [3, 5, 8, 10, 20, 30]$\times 10^7 M_\odot kpc^{-2}$

even in MOND.

The gas mass ripped from both clusters is given in B06 for a circular aperture of 80 kpc located around the sub-cluster X-ray center and an ellipse with semi-major and semi-minor axes of 250 kpc and 150 kpc around the main cluster X-ray center. Since our potentials are spherical we use a circle instead of an ellipse with the same area. The gas masses within apertures of 100kpc are given in C06 and these are consistent with the values given in B06.

In order to match the observed X-ray gas mass, which is a minor contributor to the lensing map, we use the asymmetry in the calculated surface density to subtract off all the DM and galaxies in the system. The key here is to notice the symmetry of galaxies (and likely DM) around the dashed line joining the centres of the two galaxy clusters (cf. Fig. 1 upper panel). If we fold the map around this axis of symmetry, and subtract the lower map from the upper part we should be left with cluster as it lies quite close to the axis of symmetry and thus much gas is cancelled out by other gas. For GR only we can directly compare the gas corresponding to the potential and that calculated by our subtraction method. For the main cluster within the 180kpc aperture, we find integration of the surface density gives $2.32\times10^13 M_\odot$, whereas our subtraction gives $1.97\times10^13 M_\odot$ less than a 15% difference. For the 100kpc aperture around the sub cluster we find $5.7\times10^12 M_\odot$ from integration and $3.3\times10^12 M_\odot$ from our subtraction. For the sub cluster there is clearly gas on both side of the symmetry axis, which causes the larger discrepancy here. As such, in MOND we can expect the gas masses to increase by similar amounts and this helps to explain the low gas masses found, especially in the sub cluster.

Exotic Species of Dark Matter or Ordinary Massive Neutrinos? As a probe of the nature of the non-baryonic particles in this system, we compute the volume density of matter as function of positions; the densest regions are

Bullet cluster (1E0657-558 ($z = 0.296$)), Angus et al. (2006)

IV. THE CONVERGENCE MAP FROM LENSING ANALYSIS

A. The κ-Map

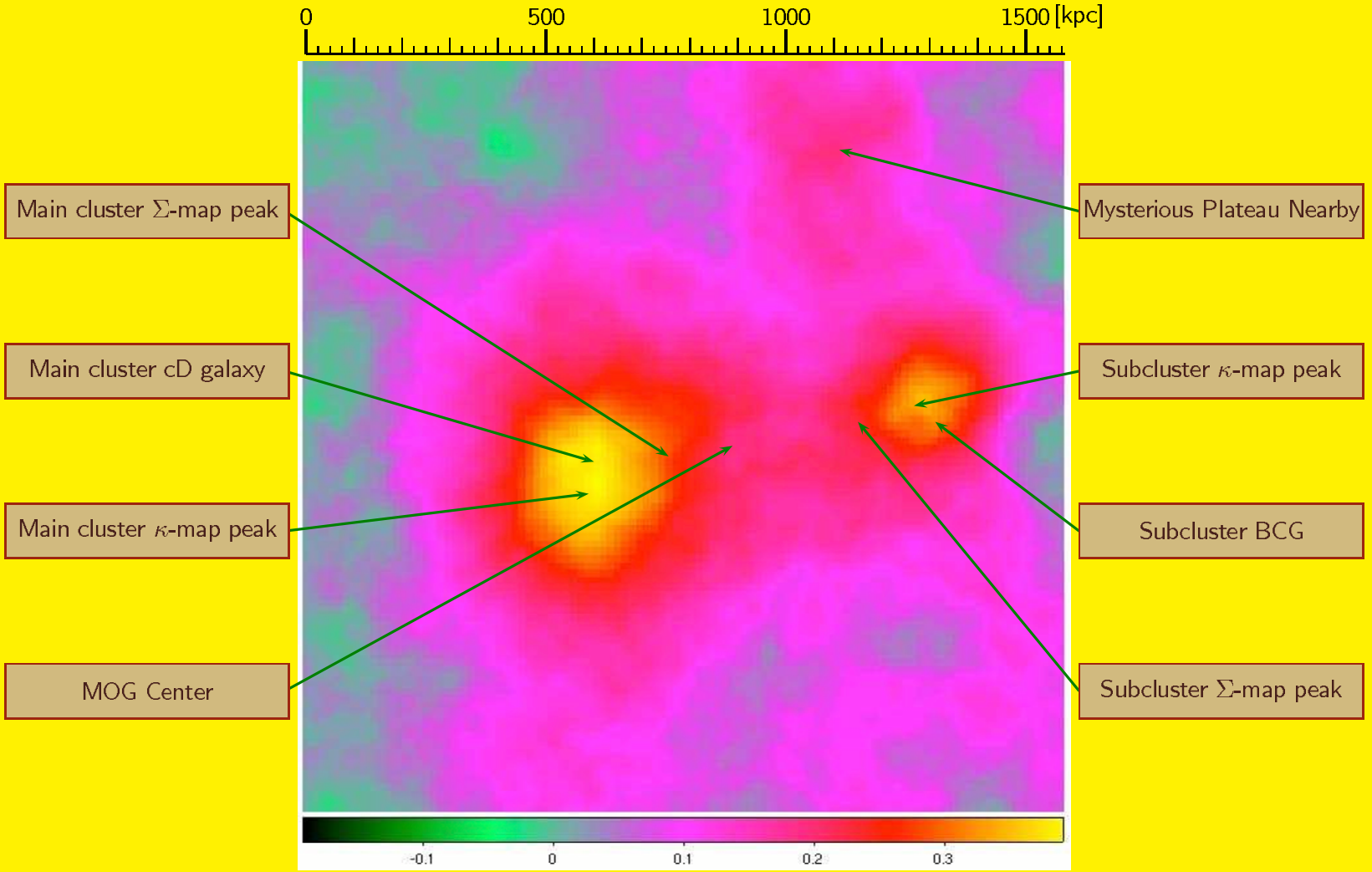

FIG. 12: The surface density κ-map reconstructed from strong and weak gravitational lensing.

Constraints on DM concentration near the GC (it is based on results of the paper by AFZ, F. De Paolis, G. Ingrosso, A.A. Nucita (PRD, 062001, 2007)

Urbain Jean Joseph Le Verrier: Neptune discovery (1846) & Mercury's anomaly (1859) (an invisible ("dark") object or a violation of the Newtonian gravity law)

A connection between cosmology and the Le Verrier's discoveries was noted out by Roman Juszkiewicz (2008).

Here I reproduce my understanding his ideas.

In 1846, analyzing trajectories of known objects (planets) and reconstructing potentials and masses and trajectories all objects in the game, Le Verrier predicted an existence of extra (initially unknown (dark)) planet, Neptune and soon afterwards the planet was detected by German

astronomer J.G. Galle. Fritz Zwicky used the same scheme leading to the introduction of dark matter (DM) concept.

Le Verrier discovered Mercury pericenter advance and explained 93% of the observed value, but a supplementary advance 38 arcseconds/century was without an explanation (later on the value was corrected such as 43 arcseconds/century).

Le Verrier's options

- A gravitational field of an invisible matter (planet, asteroids near Sun)
- A deviation from the Newtonian law
- A precision of a model is not good enough

Le Verrier (1876) analyzed information about 25 transits of Vulcan (according to his opinion 19 transits were reliable) and predicted a transit in March 1877 (the planet was not observed). Le Verrier died on 23 September 1877.

Similarly to cosmological DM and DE problems now, different options were considered such as an existence of an extra planet between the Sun

and Mercury (the Vulcan's prediction), a modification mass of Venus by more than 10% and modification of the Newton gravity law (for example, such as Newcomb's modification (1895) of the Newton's law such as $1/r^n$ ($n = 2.0000001574$ for $d\tilde{\omega}/century = 42.34''$, earlier Hall (1894) used $n = 2.00000016$ for $d\tilde{\omega}/century = 43''$).

Exempl. 3. Aſſumentes m & n pro quibuſvis indicibus dignitatum Altitudinis, & b, c pro numeris quibuſvis datis, ponamus vim centripetam eſſe ut $\frac{bA^m + cA^n}{A\,cub.}$, id eſt ut $\frac{b \text{ in } \overline{T-X}^m + c \text{ in } \overline{T-X}^n}{A\,cub.}$ ſeu (per eandem Methodum noſtram Serierum convergentium) ut $\frac{bT^m - mbXT^{m-1} + \frac{mm-m}{2} bX^2T^{m-2} + cT^n - ncXT^{n-1} + \frac{nn-n}{2} cX^2T^{n-2} \&c.}{A\,Cub.}$ & collatis numeratorum terminis, fiet $RGq. - RFq. + TFq.$ ad $bT^m + cT^n$, ut $-Fq.$ ad $-mbT^{m-1} - ncT^{n-1} + \frac{mm-m}{2} XT^{m-2} + \frac{nn-n}{2} XT^{n-2}$ &c. Et ſumendo rationes ultimas quæ prodeunt ubi orbes ad formam circularem accedunt, fit $Gq.$ ad $bT^{m-1} + cT^{n-1}$, ut $Fq.$ ad $mbT^{m-1} + ncT^{n-1}$, & viciſſim $Gq.$ ad $Fq.$ ut $bT^{m-1} + cT^{n-1}$ ad $mbT^{m-1} + ncT^{n-1}$. Quæ proportio, exponendo altitudinem maximam CV ſeu T Arithmetice per unitatem, fit $Gq.$ ad $Fq.$ ut $b + c$ ad $mb + nc$, adeoq; ut 1 ad $\frac{mb+nc}{b+c}$. Unde eſt G ad F, id eſt angulus VCp ad angulum VCP, ut 1 ad $\sqrt{\frac{mb+nc}{b+c}}$. Et propterea cum angulus VCP inter Apſidem ſummam & Apſidem imam in Ellipſi immobili ſit 180 *gr.* erit angulus VCp inter eaſdem Apſides, in Orbe quem corpus vi centripeta quantitati $\frac{bA^m + cA^n}{A\,cub.}$ proportionali deſcribit, æqualis angulo graduum $180\sqrt{\frac{b+c}{mb+nc}}$. Et eodem argumento ſi vis centripeta ſit ut $\frac{bA^m - cA^n}{A\,cub.}$, angulus inter Apſides invenietur $180\sqrt{\frac{b-c}{mb-nc}}$ graduum. Nec ſecus reſolvetur Problema in caſibus

30

I. Newton (Principia) considered a generalization of a gravitational force

$$F = \frac{br^p + cr^m}{r^3}, \tag{1}$$

then

$$d\tilde{\omega} = 2\pi\sqrt{\left|\frac{b-c}{mb-pc}\right|}. \tag{2}$$

Therefore, for $p = 1$ we have

$$F = \frac{br + cr^m}{r^3}, \tag{3}$$

thus if $m \geq 2$, we have generalizations of the Newtonian force with an extra term (Clairaut, 1745; Mikkola 2008).

So Clairaut, Hall, Newcombforces are specific cases of the Newton's relation.

For $c = 0$, $F = br^{m-3}$ and

$$d\tilde{\omega} = 2\pi\sqrt{\left|\frac{b}{mb}\right|} = 2\pi\sqrt{\frac{1}{m}}, \tag{4}$$

for $m = 3 - n$ we have

$$d\tilde{\omega} = 2\pi\sqrt{\frac{1}{3-n}} \tag{5}$$

and if $n = 2 + \delta$, then

$$d\tilde{\omega} = 2\pi\sqrt{\frac{1}{1-\delta}} \approx 2\pi(1 + \delta/2) \tag{6}$$

Therefore, following the Le Verrier's way and analyzing carefully trajectories of celestial bodies we can reconstruct gravitational potentials and mass distributions governing motions of celestial bodies.

Figure 11: Urbain Jean Joseph Le Verrier (March 11, 1811 — September 23, 1877).

DM annihilation at GC

In the last years intensive searches for dark matter (DM), especially its non-baryonic component, both in galactic halos and at galaxy centers have been undertaken (see for example Bertone et al. (2005,2005a) for recent results). It is generally accepted that the most promising candidate for the DM non-baryonic component is neutralino. In this case, the γ-flux from galactic halos (and from our Galactic halo in particular) could be explained by neutralino annihilation (Gurevich et al. 1997,Bergstrom et al. 1998, Tasitsiomi et al. 2002, Stoehr et al. 2003, Prada et al. 2004,Profumo et al. 2005, Mambrini et al. 2005). Since γ-rays are detected not only from high galactic latitude, but also from the Galactic Center, there is a wide spread hypothesis (see, Evans (2004) for a discussion) that a DM concentration might be present at the Galactic Center. In this case the Galactic Center could be a strong source of γ-rays and neutrinos (Bouquet 1989, Stecker

1988, Berezinsky et al. 1994, Bergstrom et al. 1998, Bertone et al. 2004, Gnedin et al. 2004,Bergstrom et al. 2005, Horns 2005, Bertone et al. 2005) due to DM annihilation. Since it is also expected that DM forms spikes at galaxy centers (Gondolo & Silk 1999, Ullio et al. 2001, Merritt et al. 2003) the γ-ray flux from the Galactic Center should increase significantly in that case.

At the same time, progress in monitoring bright stars near the Galactic Center have been reached recently (Genzel et al. 2003,Ghez et al. 2003, Ghez et al. 2005). The astrometric limit for bright stellar sources near the Galactic Center with 10 meter telescopes is today $\delta\theta_{10} \sim 1$ mas and the Next Generation Large Telescope (NGLT) will be able to improve this number at least down to $\delta\theta_{30} \sim 0.5$ mas (Weinberg et al. 2005) or even to $\delta\theta_{30} \sim 0.1$ mas (Weinberg et al. 2005) in the K-band. Therefore, it will be possible to measure the proper motion for about ~ 100 stars with astrometric errors several times smaller than errors in current observations.

The aim of this talk is to constrain the parameters of the DM distribution possible present around the Galactic Center by considering the induced apoastron shift due to the presence of this DM sphere and either available data obtained with the present generation of telescopes (the so called $conservative$ limit) and also expectations from future NGLT observations or with other advanced observational facilities.

Celestial mechanics of S2 like stars for BH+cluster (A.A. Nucita, F. De Paolis, G. Ingrosso, A. Qadir, AFZ, PASP, v. 119, p. 349 (2007))

GR predicts that orbits about a massive central body suffer periastron shifts yielding $rosette$ shapes. However, the classical perturbing effects of other objects on inner orbits give an opposite shift. Since the periastron advance depends strongly on the compactness of the central body, the detection of such an effect may give information about the nature of the central body itself. This would apply for stars orbiting close to the GC, where there is a "dark object", the black hole hypothesis being the most natural explanation of the observational data. A cluster of stars in the vicinity of the GC (at a distance < 1 arcsec) has been monitored by ESO and Keck teams for several years.

For a test particle orbiting a Schwarzschild black hole of mass $M_{\rm BH}$, the periastron shift is given by (see e.g. Weinberg, 1972)

$$\Delta\phi_S \simeq \frac{6\pi G M_{BH}}{d(1-e^2)c^2} + \frac{3(18+e^2)\pi G^2 M_{BH}^2}{2d^2(1-e^2)^2c^4} \ , \tag{7}$$

d and e being the semi-major axis and eccentricity of the test particle orbit, respectively. For a rotating black hole with spin parameter $a = |\mathbf{a}| = J/GM_{\rm BH}$, the space-time is described by the Kerr metric and, in the most favorable case of equatorial plane motion (**(a,v)** $= 0$), the shift is given by (Boyer and Price (1965))

$$\Delta\phi_K \simeq \Delta\phi_S + \frac{8a\pi M_{BH}^{1/2} G^{3/2}}{d^{3/2}(1-e^2)^{3/2}c^3} + \frac{3a^2\pi G^2}{d^2(1-e^2)^2c^4} \ , \tag{8}$$

which reduces to eq. (7) for $a \to 0$. In the more general case, **a.v** $\neq 0$, the

expected periastron shift has to be evaluated numerically.

The expected periastron shifts (mas/revolution), $\Delta\phi$ (as seen from the center) and $\Delta\phi_E$ (as seen from Earth at the distance $R_0 \simeq 8$ kpc from the GC), for the Schwarzschild and the extreme Kerr black holes, for the S2 and S16 stars turn out to be $\Delta\phi^{S2} = 6.3329 \times 10^5$ and 6.4410×10^5 and $\Delta\phi_E^{S2} = 0.661$ and 0.672 respectively, and $\Delta\phi^{S16} = 1.6428 \times 10^6$ and 1.6881×10^6 and $\Delta\phi_E^{S16} = 3.307$ and 3.399 respectively. Recall that

$$\Delta\phi_E = \frac{d(1+e)}{R_0}\Delta\phi_{S,K} \ . \tag{9}$$

Notice that the differences between the periastron shifts for the Schwarzschild and the maximally rotating Kerr black hole is at most 0.01 mas for the S2 star and 0.009 mas for the S16 star. In order to make these measurements with the required accuracy, one needs to know the S2 orbit with a precision of at least 10 μas.

The star cluster surrounding the central black hole in the GC could be sizable. At least 17 members have been observed within 15 mpc up to now (Ghez et al. (2005)). However, the cluster mass and density distribution, that is to say its mass and core radius, is still unknown. The presence of this cluster affects the periastron shift of stars orbiting the central black hole. The periastron advance depends strongly on the mass density profile and especially on the central density and typical length scale.

We model the stellar cluster by a Plummer model density profile (Binney & Tremaine (1987))

$$\rho_{CL}(r) = \rho_0 f(r) \ , \qquad \text{with} \qquad f(r) = \left[1 + \left(\frac{r}{r_c}\right)^2\right]^{-\alpha/2} \ , \quad (10)$$

where the cluster central density ρ_0 is given by

$$\rho_0 = \frac{M_{CL}}{\int_0^{R_{CL}} 4\pi r^2 f(r)\, dr}\ , \tag{11}$$

R_{CL} and M_{CL} being the cluster radius and mass, respectively. According to dynamical observations towards the GC, we require that the total mass $M(r) = M_{BH} + M_{CL}(r)$ contained within $r \simeq 5 \times 10^{-3}$ pc is $M \simeq 3.67 \times 10^6\ M_\odot$. Useful information is provided by the cluster mass fraction, $\lambda_{CL} = M_{CL}/M$, and its complement, $\lambda_{BH} = 1 - \lambda_{CL}$. As one can see, the requirement given in eq. (11) implies that $M(r) \to M_{BH}$ for $r \to 0$. The total mass density profile $\rho(r)$ is given by

$$\rho(r) = \lambda_{BH} M \delta^{(3)}(\overrightarrow{r}) + \rho_0 f(r) \tag{12}$$

and the mass contained within r is

$$M(r) = \lambda_{BH} M + \int_0^r 4\pi r'^2 \rho_0 f(r') \, dr' \ . \tag{13}$$

According to GR, the motion of a test particle can be fully described by solving the geodesic equations. Under the assumption that the matter distribution is static and pressureless, the equation of motion of the test particle becomes (see e.g. Weinberg 1972))

$$\frac{d\mathbf{v}}{dt} \simeq -\nabla(\Phi_N + 2\Phi_N^2) + 4\mathbf{v}(\mathbf{v}\cdot\nabla)\Phi_N - v^2\nabla\Phi_N \ . \tag{14}$$

For the S2 star, d and e given in the literature are 919 AU and 0.87 respectively. They yield the orbits of the S2 star for different values of the

black hole mass fraction λ_{BH} shown in Figure 12. The Plummer model parameters are $\alpha = 5$, core radius $r_c \simeq 5.8$ mpc. Note that in the case of $\lambda_{BH} = 1$, the expected (prograde) periastron shift is that given by eq. (7), while the presence of the stellar cluster leads to a retrograde periastron shift. For comparison, the expected periastron shift for the S16 star is given in Figure 23. In the latter case, the binary system orbital parameters were taken from Schödel et al. (2003)) assuming also for the S16 mass a conservative value of $\simeq 10$ $M_\odot$.

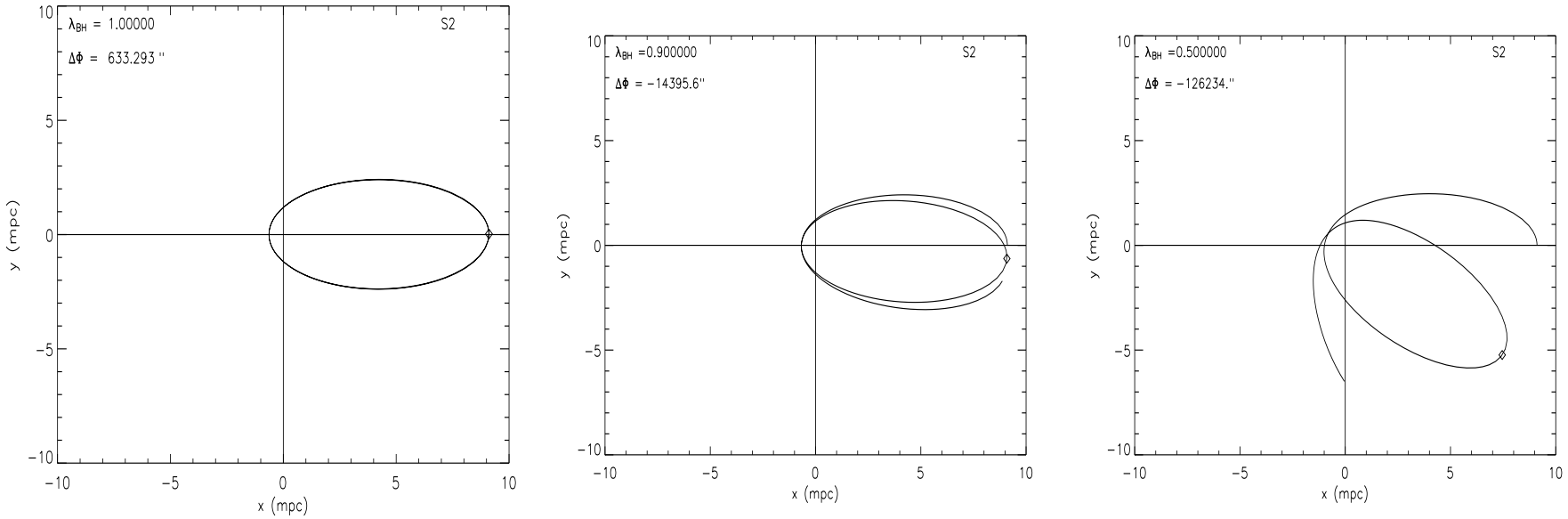

Figure 12: Post Newtonian orbits for different values of the black hole mass fraction λ_{BH} are shown for the S2 star (upper panels). Here, we have assumed that the Galactic central black hole is surrounded by a stellar cluster whose density profile follows a Plummer model with $\alpha = 5$ and a core radius $r_c \simeq 5.8$ mpc. The periastron shift values in each panel is given in arcseconds.

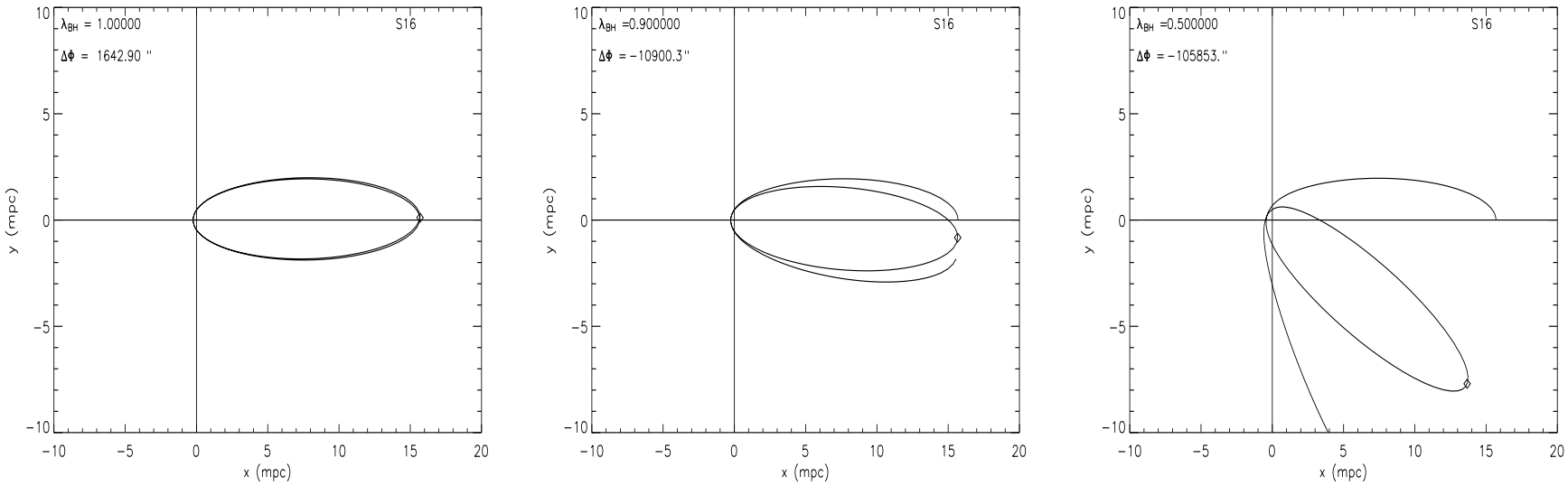

Figure 13: The same as in Figure 12 but for the S16–Sgr A* binary system. In this case, the binary system orbital parameters were taken from Ghez et al. (2005) assuming for the S16 mass a conservative value of $\simeq 10$ $M_\odot$.

The mass concentration at the Galactic Center

Recent advancements in infrared astronomy are allowing to test the scale of the mass profile at the center of our galaxy down to tens of AU. With the Keck 10 m telescope, the proper motion of several stars orbiting the Galactic Center black hole have been monitored and almost entire orbits, as for example that of the S2 star, have been measured allowing an unprecedent description of the Galactic Center region. Measurements of the amount of mass $M(< r)$ contained within a distance r from the Galactic Center are continuously improved as more precise data are collected. Recent observations (Ghez et al. (2003)) extend down to the periastron distance ($\simeq 3 \times 10^{-4}$ pc) of the S16 star and they correspond to a value of the enclosed mass within $\simeq 3 \times 10^{-4}$ pc of $\simeq 3.67 \times 10^{6}$ $M_{\odot}$. Several authors have used these observations to model the Galactic Center mass concentration. Here and in the following, we use the three component

model for the central region of our galaxy based on estimates of enclosed mass given by Ghez et al (2003, 2005) recently proposed by Hall and Gondolo (2006). This model is constituted by the central black hole, the central stellar cluster and the DM sphere (made of WIMPs), i.e.

$$M(< r) = M_{BH} + M_*(< r) + M_{DM}(< r) \ , \tag{15}$$

where M_{BH} is the mass of the central black hole Sagittarius A*. For the central stellar cluster, the empirical mass profile is

$$M_*(< r) = \begin{cases} M_* \left(\frac{r}{R_*}\right)^{1.6} \ , & r \leq R_* \\ \\ M_* \left(\frac{r}{R_*}\right)^{1.0} \ , & r > R_* \end{cases} \tag{16}$$

with a total stellar mass $M_* = 0.88 \times 10^6$ M$_\odot$ and a size $R_* = 0.3878$ pc.

As far as the mass profile of the DM concentration is concerned, Hall & Gondolo (2006) have assumed a mass distribution of the form

$$M_{DM}(< r) = \begin{cases} M_{DM}\left(\frac{r}{R_{DM}}\right)^{3-\alpha}, & r \leq R_{DM} \\ M_{DM}, & r > R_{DM} \end{cases} \quad (17)$$

M_{DM} and R_{DM} being the total amount of DM in the form of WIMPs and the radius of the spherical mass distribution, respectively.

Hall and Gondolo (2006) discussed limits on DM mass around the black hole at the Galactic Center. It is clear that present observations of stars around the Galactic Center do not exclude the existence of a DM sphere with mass $\simeq 4 \times 10^6 M_\odot$, well contained within the orbits of the known stars, if its radius R_{DM} is $\lesssim 2 \times 10^{-4}$ pc (the periastron distance of the S16 star in the more recent analysis (Ghez et al. 2005)). However, if one

considers a DM sphere with larger radius, the corresponding upper value for M_{DM} decreases (although it tends again to increase for extremely extended DM configurations with $R_{DM} \gg 10$ pc). In the following, we will assume for definiteness a DM mass $M_{DM} \sim 2 \times 10^5 M_\odot$, that is the upper value for the DM sphere (Hall & Gondolo (2006)) within an acceptable confidence level in the range $10^{-3} - 10^{-2}$ pc for R_{DM}. As it will be clear in the following, we emphasize that even a such small value for the DM mass (that is about only 5% of the standard estimate $3.67 \pm 0.19 \times 10^6\ M_\odot$ for the dark mass at the Galactic Center (Ghez et al. 2005)) may give some observational signatures.

Evaluating the S2 apoastron shift [1] as a function of R_{DM}, one can further constrain the DM sphere radius since even now we can say that there is no evidence for negative apoastron shift for the S2 star orbit at the

[1] We want to note that the periastron and apoastron shifts $\Delta\Phi$ as seen from the orbit center have the same value whereas they have different values as seen from Earth (see Eq. (21)). When we are comparing our results with orbit reconstruction from observations we refer to the apoastron shift as seen from Earth.

level of about 10 mas (Genzel et al. 2003). In addition, since at present the precision of the S2 orbit reconstruction is about 1 mas, we can say that even without future upgrades of the observational facilities and simply monitoring the S2 orbit, it will be possible within about 15 years to get much more severe constraints on R_{DM}.

Moreover, observational facilities will allow in the next future to monitor faint infrared objects at the astrometric precision of about 10 μas (Eisenhauer et al. 2005) and, in this case, previous estimates will be sensibly improved since it is naturally expected to monitor eccentric orbits for faint infrared stars closer to the Galactic Center with respect to the S2 star.

In Fig. 22, the mass profile $M(< r)$ (Ghez et al. 2003) obtained by using observations of stars nearby the Galactic Center is shown (solid line). The dotted line represents the stellar mass profile as given in Eq. (16), while the dashed lines are for DM spheres with mass $M_{DM} \simeq 2 \times 10^5$ M$_\odot$ and

radii $R_{DM} = 10^{-3}$ and 10^{-2} pc, respectively.

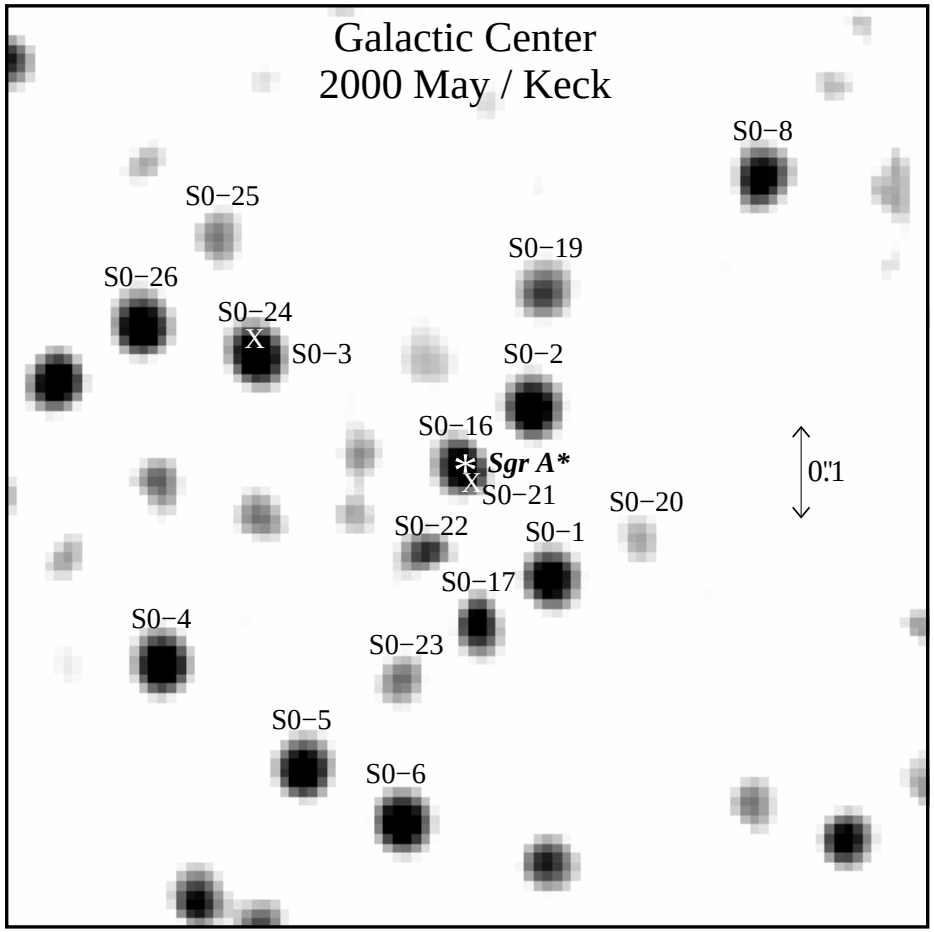

Figure 14: The S2 like star locations near the Black Hole at the Galactic Center (Ghez et al. 2005).

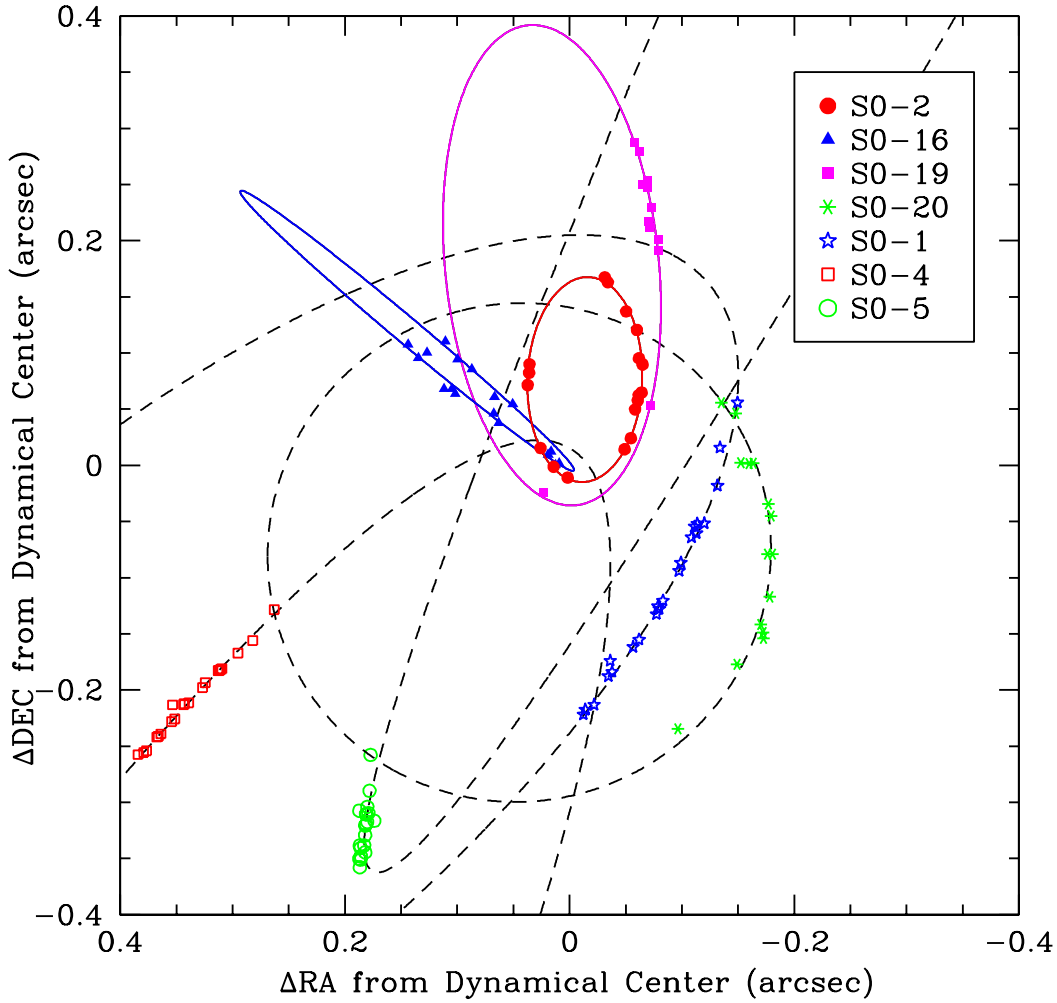

Figure 15: The S2 like star trajectories near the Black Hole at the Galactic Center (Ghez et al (2005)).

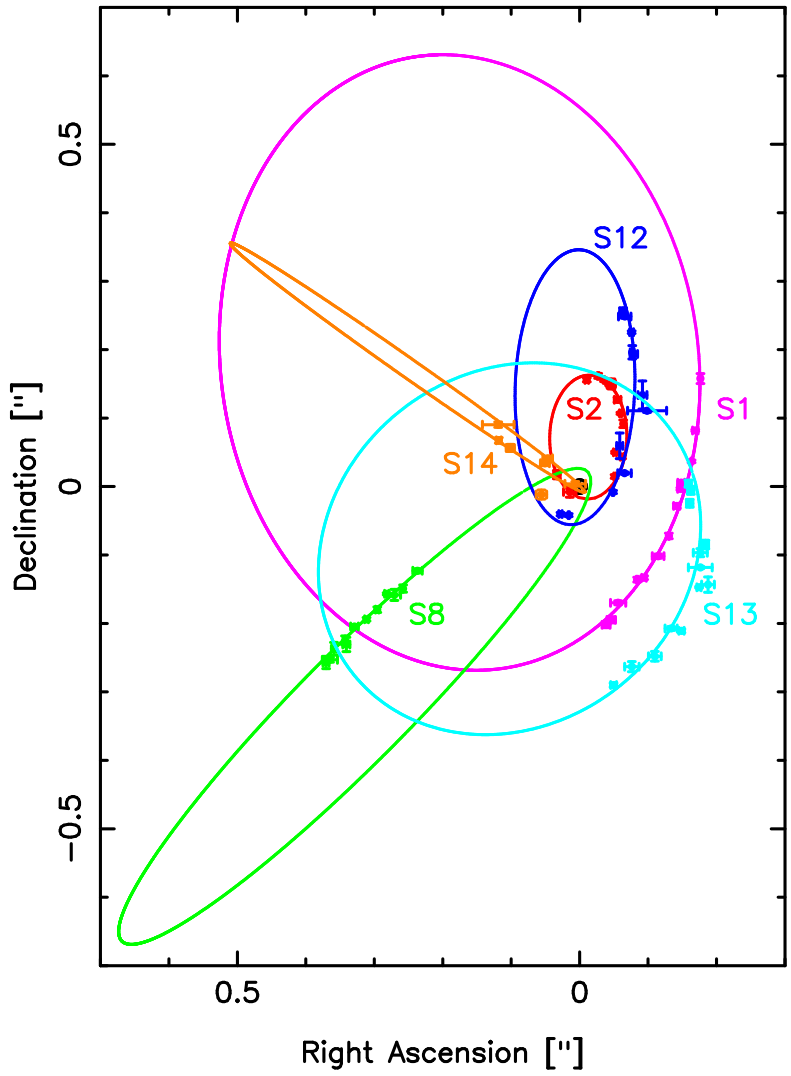

Figure 16: The S2 like star trajectories near the Black Hole at the Galactic Center (Schodel et al (2003)).

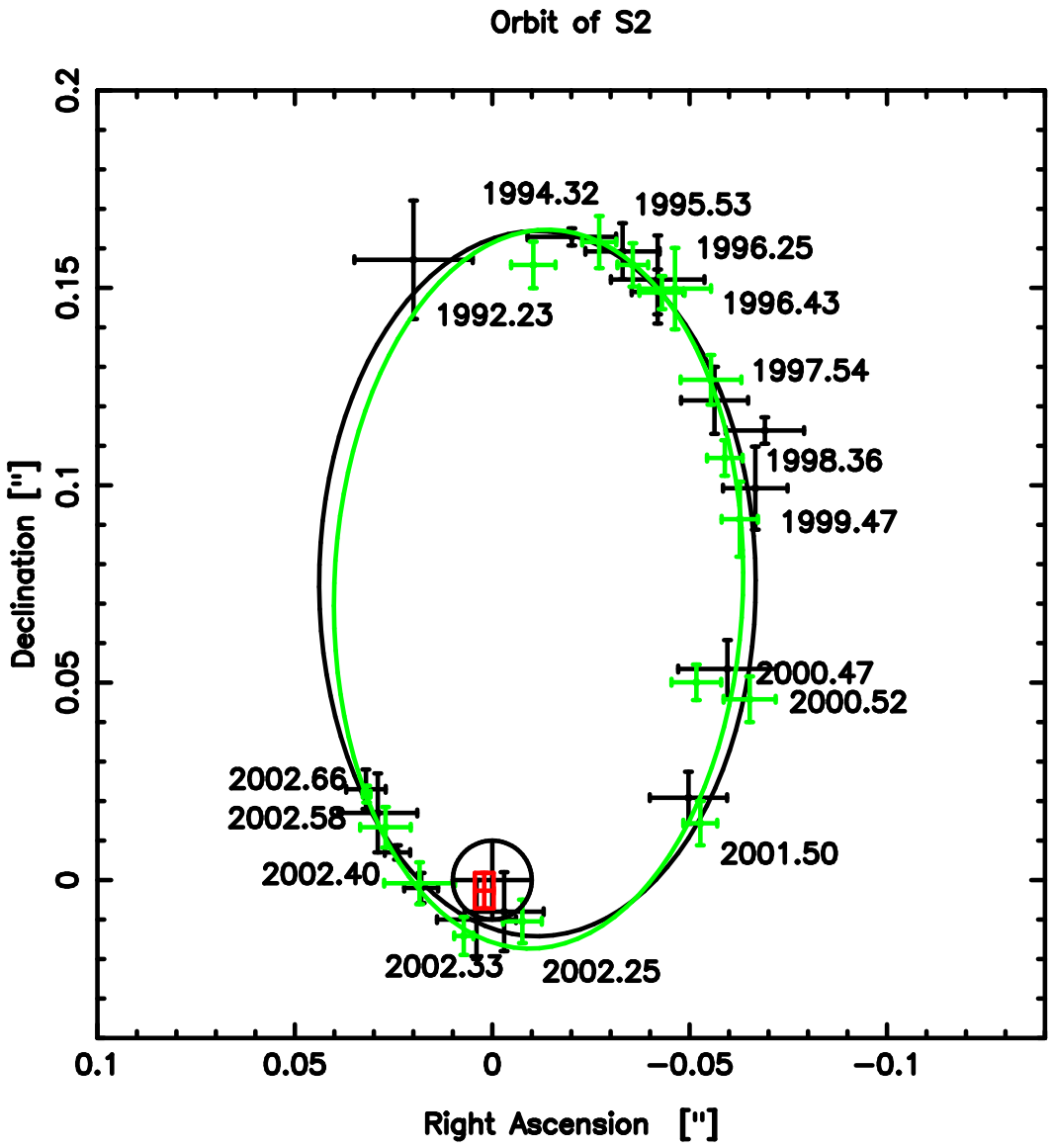

Figure 17: The S2 star trajectory near the Black Hole at the Galactic Center (Schodel et al (2003)).

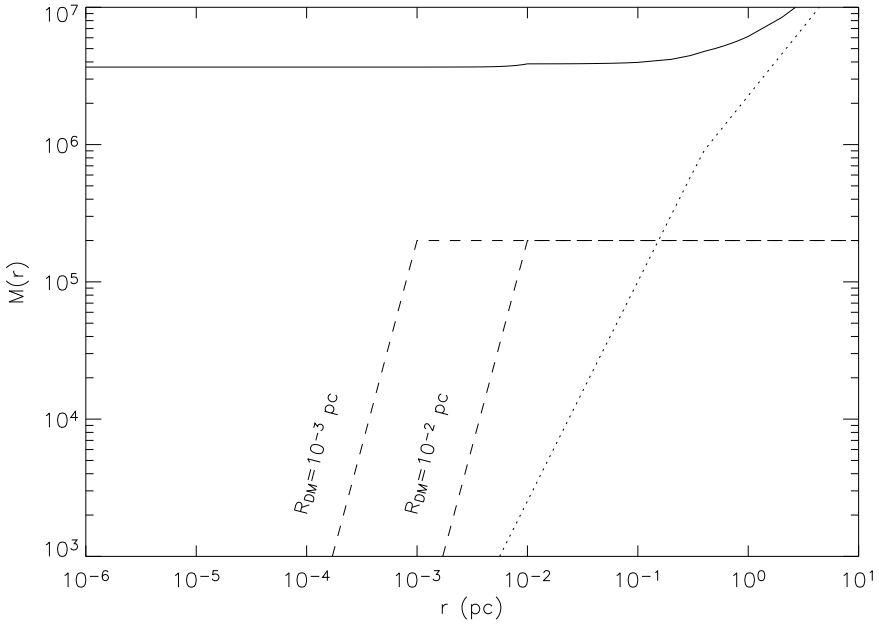

Figure 18: The mass $M(< r)$ obtained in (Ghez et al. 2003) from observations of stars at the Galactic Center is shown (solid line). The dotted line represents the stellar mass profile as given in Eq. (16), while the dashed lines are for DM spheres with radii $R_{DM} = 10^{-3}$ and 10^{-2} pc and mass $M_{DM} \simeq 2 \times 10^5$ $M_\odot$, that corresponds to some acceptable estimate for the upper limit of M_{DM} from Hall and Gondolo (2006).

In the following section, we study the motion of stars as a consequence of the gravitational potential $\Phi(r)$ due the mass profile given in Eq. (15). As usual, the gravitational potential can be evaluated as

$$\Phi(r) = -G \int_r^\infty \frac{M(r')}{r'^2}\, dr' \ . \tag{18}$$

For convenience, in Fig. 19 the gravitational potential due to the total mass (solid line) contained within r is given as function of the galactocentric distance. For comparison, the contributions due to the single mass components, i.e. central black hole, stellar cluster and DM sphere, are also shown.

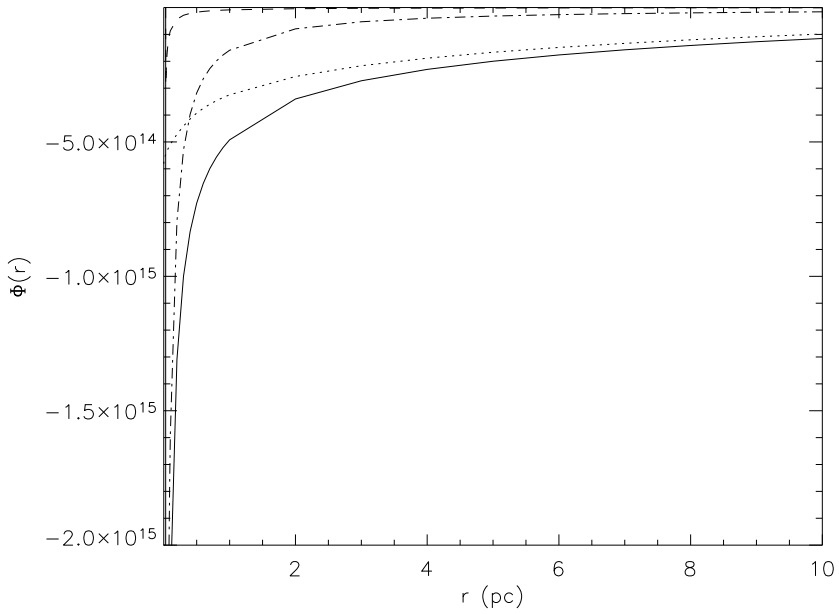

Figure 19: The gravitational potential $\Phi(r)$ (solid line) in cgs units as a function of the galactocentric distance r as due to the mass $M(r)$ in Eq.(15) is shown. For comparison, also the gravitational potentials due to the single mass components, i.e. black hole (dashed line), stellar cluster (dot-dashed line) and DM (dotted line), are also given. Here we assume that DM mass $M_{DM} \simeq 2 \times 10^5$ $M_\odot$ and radius $R_{DM} = 10^{-3}$ pc.

Apoastron Shift Constraints

According to GR, the motion of a test particle can be fully described by solving the geodesic equations. Under the assumption that the matter distribution is static and pressureless, the equations of motion at the first post-Newtonian (PN) approximation become (see e.g. (Fock 1961, Weinberg 1972, Rubilar & Eckart 2001))

$$\frac{d\mathbf{v}}{dt} \simeq -\nabla(\Phi_N + 2\Phi_N^2) + 4\mathbf{v}(\mathbf{v}\cdot\nabla)\Phi_N - v^2\nabla\Phi_N \ . \qquad (19)$$

We note that the PN-approximation is the first relativistic correction from which the apoastron advance phenomenon arises. In the case of the S2 star, the apoastron shift as seen from Earth (from Eq. (21)) due to the presence of a central black hole is about 1 mas, therefore not directly

detectable at present since the available precision in the apoastron shift is about 10 mas (but it will become about 1 mas in 10–15 years even without considering possible technological improvements). It is also evident that higher order relativistic corrections to the S2 apoastron shift are even smaller and therefore may be neglected at present, although they may become important in the future.

As it will be discussed below, the Newtonian effect due to the existence of a sufficiently extended DM sphere around the black hole may cause a apoastron shift in the opposite direction with respect to the relativistic advance due to the black hole. Therefore, we have considered the two effects comparing only the leading terms.

For the DM distribution at the Galactic Center we follow Eq. (17) as done in Hall & Gondolo (2006). Clearly, if in the future faint infrared stars (or spots) closer to the black hole with respect to the S2 star will be monitored (Eisenhauer, (2005)), this simplified model might well not hold

and higher order relativistic corrections may become necessary.

For a spherically symmetric mass distribution (such as that described above) and for a gravitational potential given by Eq. (18), Eq. (19) may be rewritten in the form (see for details Rubilar & Eckart (2001))

$$\frac{d\mathbf{v}}{dt} \simeq -\frac{GM(r)}{r^3}\left[\left(1+\frac{4\Phi_N}{c^2}+\frac{v^2}{c^2}\right)\mathbf{r}-\frac{4\mathbf{v}(\mathbf{v}\cdot\mathbf{r})}{c^2}\right], \qquad (20)$$

r and **v** being the vector radius of the test particle with respect to the center of the stellar cluster and the velocity vector, respectively. Once the initial conditions for the star distance and velocity are given, the rosetta shaped orbit followed by a test particle can be found by numerically solving the set of ordinary differential equations in eq. (20).

In Fig. 12, as an example, assuming that the test particle orbiting the Galactic Center region is the S2 star, we show the Post Newtonian orbits

obtained by the black hole only, the black hole plus the stellar cluster and the contribution of two different DM mass density profiles. In each case the S2 orbit apoastron shift is given. As one can see, for selected parameters for DM and stellar cluster masses and radii the effect of the stellar cluster is almost negligible while the effect of the DM distribution is crucial since it enormously overcome the shift due to the relativistic precession. Moreover, as expected, its contribution is opposite in sign with respect to that of the black hole (Nucita et al. (2007)).

We note that the expected apoastron (or, equivalently, periastron) shifts (mas/revolution), $\Delta\Phi$ (as seen from the center) and the corresponding values $\Delta\phi_E^{\pm}$ as seen from Earth (at the distance $R_0 \simeq 8$ kpc from the GC) are related by

$$\Delta\phi_E^{\pm} = \frac{d(1 \pm e)}{R_0}\Delta\Phi, \tag{21}$$

where with the sign $\pm$ are indicated the shift angles of the apoastron $(+)$

and periastron (-), respectively. The S2 star semi-major axis and eccentricity are $d = 919$ AU and $e = 0.87$ (Ghez et al. 2005).

In Fig. 24, the S2 apoastron shift as a function of the DM distribution size R_{DM} is given for $\alpha = 0$ and $M_{DM} \simeq 2 \times 10^5$ $M_\odot$. Taking into account that the present day precision for the apoastron shift measurements is of about 10 mas, one can say that the S2 apoastron shift cannot be larger than 10 mas. Therefore, any DM configuration that gives a total S2 apoastron shift larger than 10 mas (in the opposite direction due to the DM sphere) is excluded. The same analysis is shown in Figs. 25 and 26 for two different values of the DM mass distribution slope, i.e. $\alpha = 1$ and $\alpha = 2$, respectively. In any case, we have calculated the apoastron shift for the S2 star orbit assuming a total DM mass $M_{DM} \simeq 2 \times 10^5$ $M_\odot$. As one can see by inspecting Figs. 24-26, the upper limit of about 10 mas on the S2 apoastron shift may allow to conclude that DM radii in the range about $10^{-3} - 10^{-2}$ pc are excluded by present observations.

We notice that the results of the present analysis allows to further constrain the results (Hall and Gondolo 2006) who have concluded that if the DM sphere radius is in the range $10^{-3} - 1$ pc, configurations with DM mass up to $M_{DM} = 2 \times 10^5\ M_\odot$ are acceptable. The present analysis shows that DM configurations of the same mass are acceptable only for R_{DM} out the range between $10^{-3} - 10^{-2}$ pc, almost irrespectively of the α value.

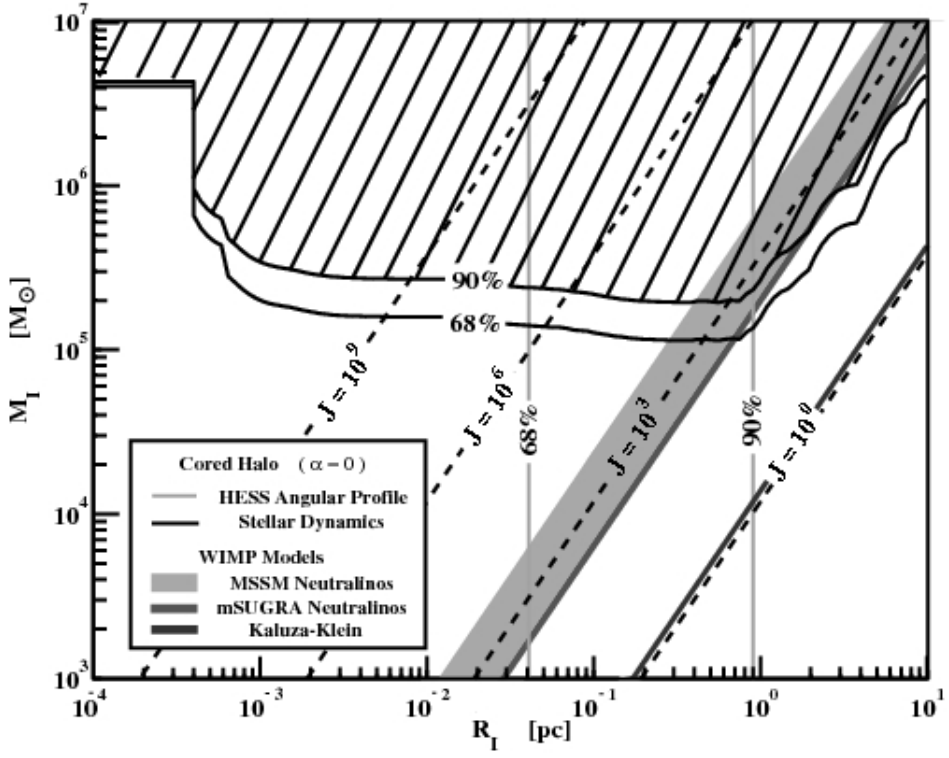

Figure 20: An allowed region for DM distribution from S2 like star trajectories near the Black Hole at the Galactic Center (Hall and Gondolo (2006)).

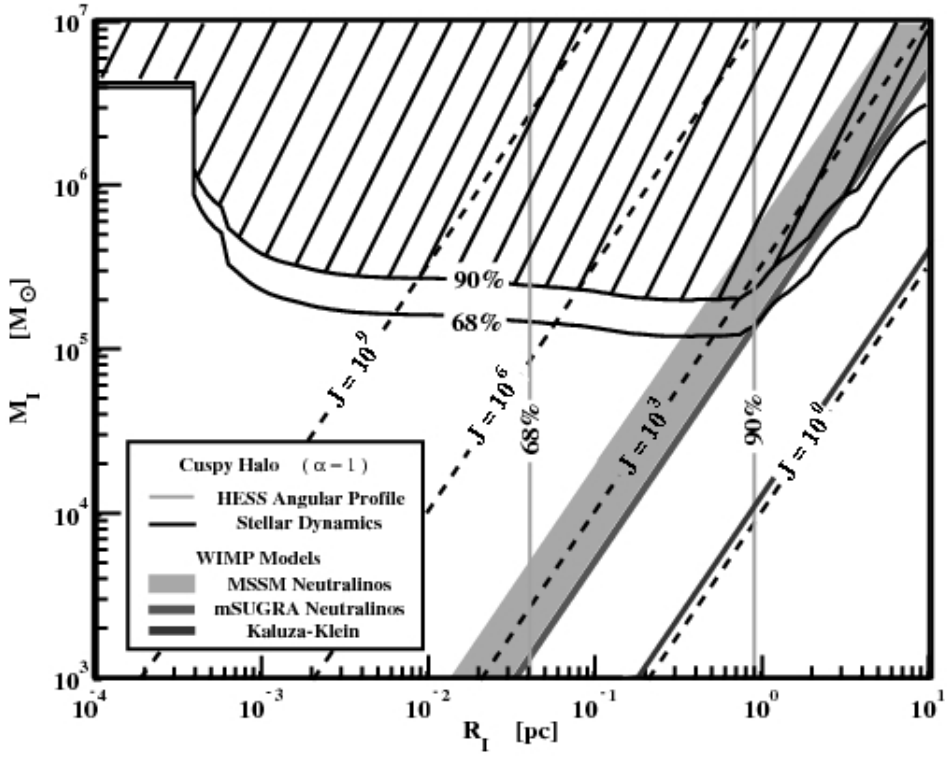

Figure 21: An allowed region for DM distribution from S2 like star trajectories near the Black Hole at the Galactic Center (Hall and Gondolo (2006).

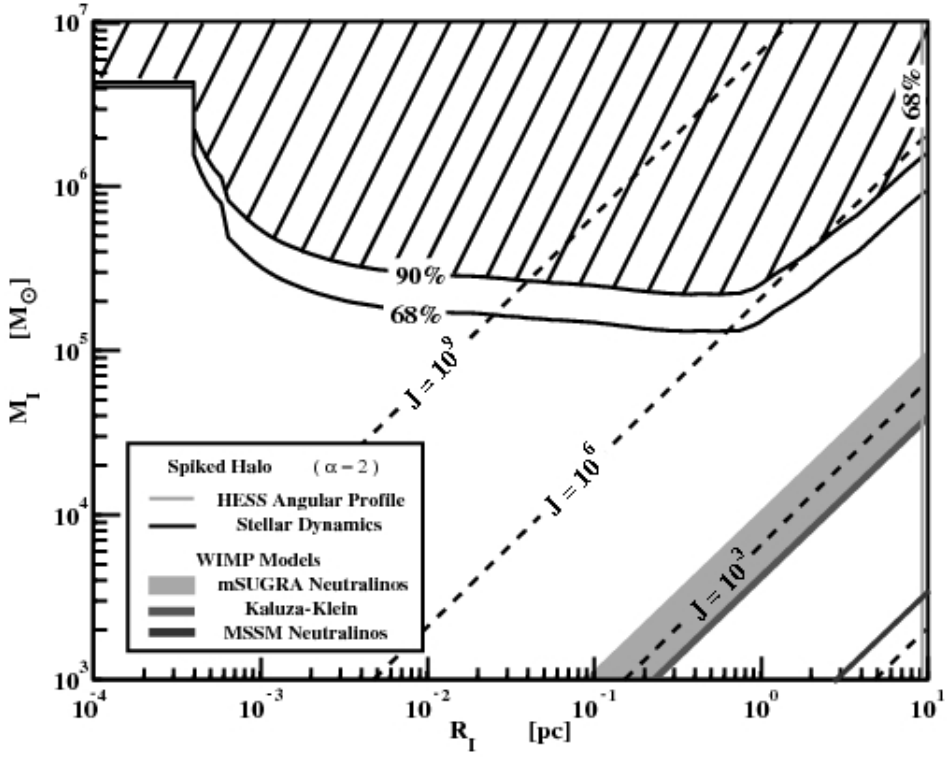

Figure 22: An allowed region for DM distribution from S2 like star trajectories near the Black Hole at the Galactic Center (Hall and Gondolo (2006).

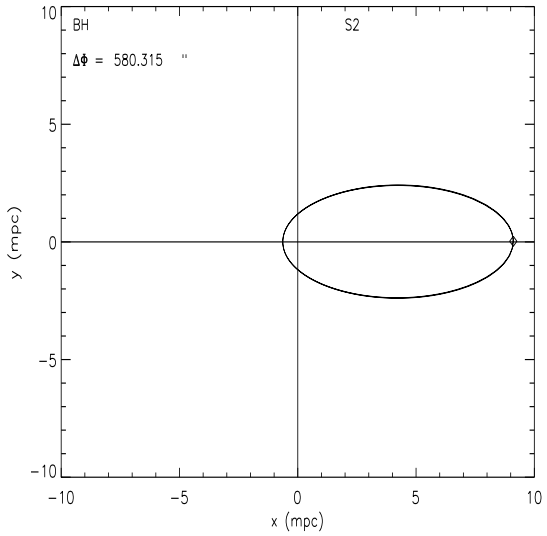
BH
S2
Δϕ = 580.315 ''
y (mpc)
x (mpc)

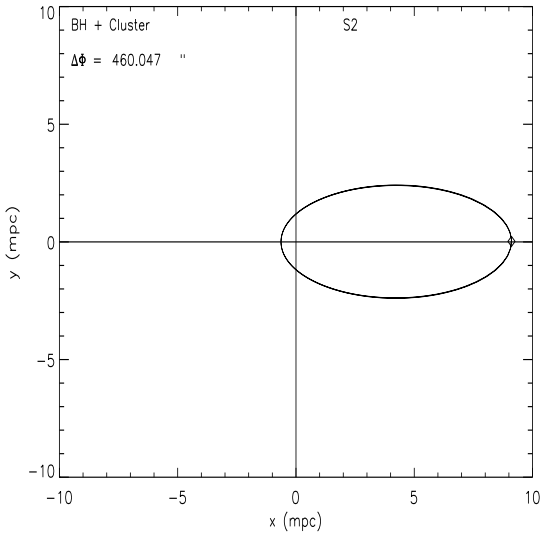
BH + Cluster
S2
Δϕ = 460.047 ''
y (mpc)
x (mpc)

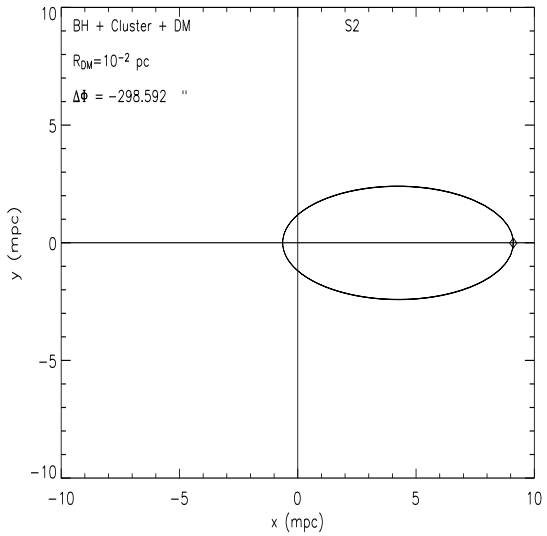
BH + Cluster + DM
S2
R_DM=10^-2 pc
Δϕ = −298.592 ''
y (mpc)
x (mpc)

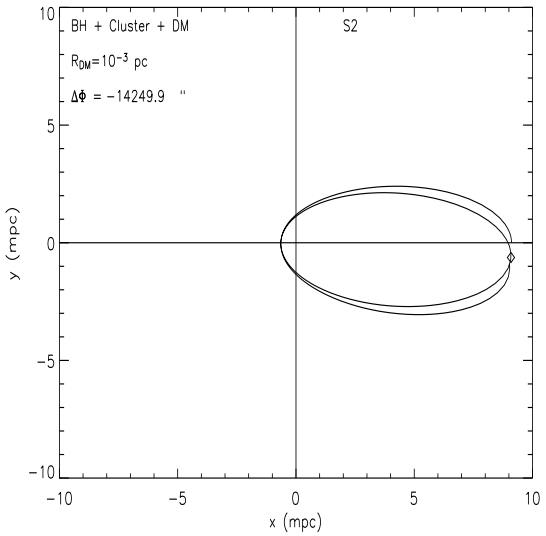
BH + Cluster + DM
S2
R_DM=10^-3 pc
Δϕ = −14249.9 ''
y (mpc)
x (mpc)

Figure 23: PN-orbits for different mass configurations at the Galactic Center. The S2 star has been considered as a test particle and its apoastron shift is indicated in each panel as $\Delta\Phi$ (in arcsec). The top-left panel shows the central black hole contribution to the S2 shift that amounts to about 580 arcsec. The top-right panels shows the combined contribution of the black hole and the stellar cluster (taken following eq. 16) to the S2 apoastron shift. In the two bottom panels the contribution due to two different DM mass-density profiles is added (as derived in eq. 17). We assume that DM mass $M_{DM} \simeq 2 \times 10^5$ $M_\odot$.

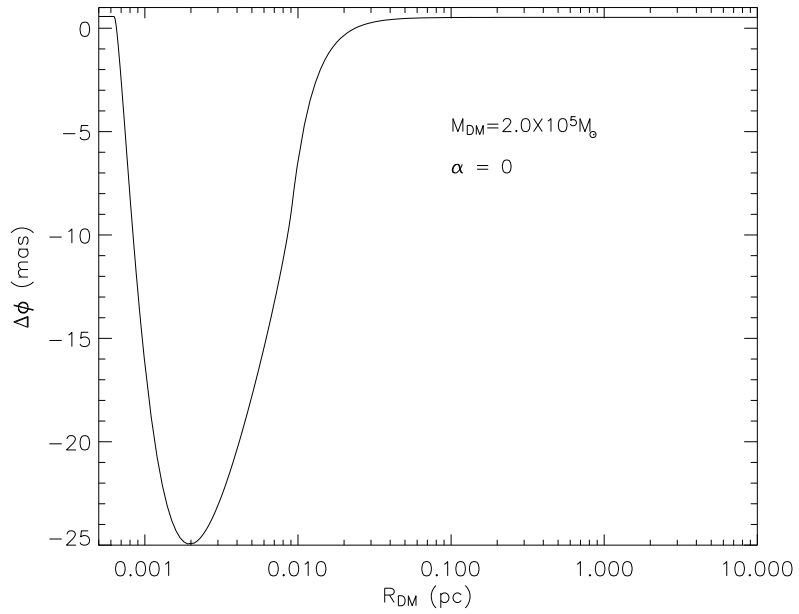

Figure 24: Apoastron shift as a function of the DM radius R_{DM} for $\alpha = 0$ and $M_{DM} \simeq 2 \times 10^5$ $M_\odot$. Taking into account present day precision for the apoastron shift measurements (about 10 mas) one can say that DM radii R_{DM} in the range $8 \times 10^{-4} - 10^{-2}$ pc are not acceptable.

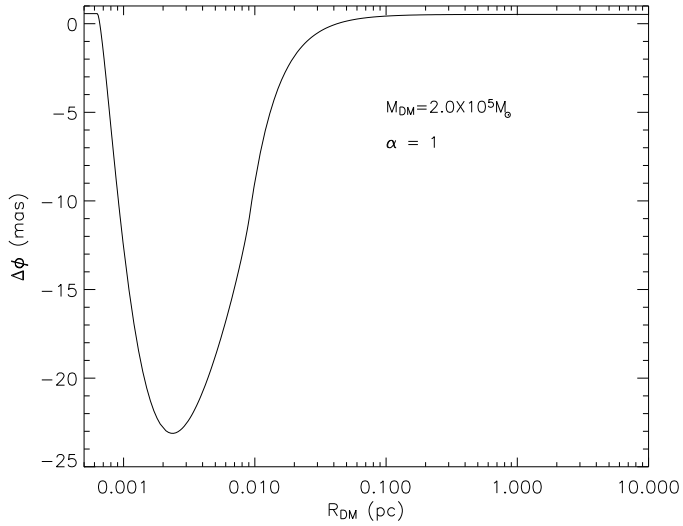

Figure 25: The same as in Fig. 24 for $\alpha = 1$ and $M_{DM} \simeq 2 \times 10^5$ $M_\odot$. As in the previous case one can say that the S2 apoastron shift put severe limits on the DM mass radii that are not acceptable in the range $9 \times 10^{-4} - 10^{-2}$ pc.

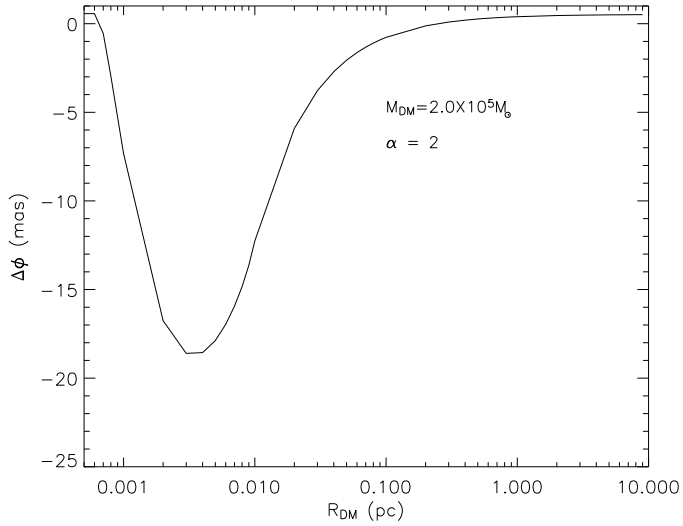

Figure 26: The same as in Fig. 24 for $\alpha = 2$ and $M_{DM} \simeq 2 \times 10^5$ $M_\odot$. As in the previous case one can say that the upper limit to the S2 apoastron shift allows to constrain the DM radius to be out the range $1.0 \times 10^{-3} - 1.1 \times 10^{-2}$ pc.

Discussion

We have considered the constraints that the upper limit (presently of about 10 mas) of the S2 apoastron shift may put on the DM configurations at the galactic center considered by Hall and Gondolo (2006).

When (in about 10-15 years, even without considering improvements in observational facilities) the precision of S2 apoastron shift will be about 1 mas (that is equal to the present accuracy in the S2 orbit reconstruction) our analysis will allow to further constrain the DM distribution parameters. In particular, the asymmetric shape of the curves in Figs. 24-26 imply that any improvement in the apoastron shift measurements will allow to extend the forbidden region especially for the upper limit for R_{DM}.

In this context, future facilities for astrometric measurements at a level

10 μas of faint infrared stars will be extremely useful (Eisenhauer 2005) and they give a chance to put even more severe constraints on DM distribution.

In addition, it is also expected to detect faint infrared stars or even hot spots (Genzel & Karas 2007) orbiting the Galactic Center. In this case, consideration of higher order relativistic corrections for an adequate analysis of the stellar orbital motion have to be taken into account.

In our considerations we adopted simple analytical expression and reliable values for R_{DM} and M_{DM} parameters following Hall & Gondolo (2006) just to illustrate the relevance of the apoastron shift phenomenon in constraining the DM mass distribution at the Galactic Center. If other models for the DM distributions are considered (see, for instance (Merritt et al. 2007) and references therein) the qualitative aspects of the problem are preserved although, of course, quantitative results on apoastron shifts may be different.

Conclusions

- Axions and neutralino look like probable candidates for DM particles
- Claims about there discoveries in direct and indirect ways have to be checked
- Present large telescopes and especially forthcoming Next Generation Large Telescope (NGLT) could be treated as a tool for an indirect detection of DM near the Galactic Center

Thank you for your attention